Original paper

The petrostructural characteristics and $^{207}Pb/^{206}Pb$ zircon data from the Ngomedzap-Akongo area (Nyong complex, SW-Cameroon)

Sébastien OWONA[1,3*], Joseph MVONDO ONDOA[2], Marion TICHOMIROWA[3], Georges Emmanuel EKODECK[1]

[1] *Department of Earth Sciences, Faculty of Science, University of Douala, P.O. Box: 24157, Douala, Cameroon; owonas@univ-douala.com*
[2] *Department of Earth Sciences, Faculty of Science, University of Yaounde I, P.O. Box: 812, Yaounde, Cameroon*
[3] *Institute of Mineralogy, TU-Bergakademie Freiberg, Freiberg D–09596, Germany*
[*] *Corresponding author*

Herein, we constrain the Ngomedzap–Akongo geodynamic evolution in the eastern part of the Nyong complex (NyC) in SW Cameroon that belongs to the Paleoproterozoic West Central African Fold Belt (WCAF) through petrostructural field observations, laboratory analyses, and $^{207}Pb/^{206}Pb$ zircon geochronology. It consists of magnetite bearing quartzite, metagranodiorite, metaanorthosite, metagabbro, and metasyenites that have recorded a polyphase D_1–D_3 deformation. D_1, likely a pure shear-type, has been strongly overprinted by the D_2 transpression flow regime that emplaced the Nyong tectonic nappe, transported top – to the East onto the Congo shield. This nappe is dissected by D_3 blastomylonitic shear--zones. Both the D_2 and D_3 have controlled the actual geometry of the Nyong belt, later crosscut by D_4 multiple brittle tectonic styles, likely post-orogenic. Zircon geochronology yielded $^{207}Pb/^{206}Pb$ zircon geochronology protolith Archean mean ages of 2764 ± 26 Ma (*MSWD* = 0.81) in metagranodiorite; 2816 ± 34 Ma (*MSWD* = 1.3) and 2789 ± 13 Ma (*MSWD* = 0.28) in metasyenites. These new data corroborate old ones and, together, document the Archean origin of the NyC as details of the Nyong fold-and-thrust belts that of WCAFB and South American homologous due to the colliding Congo--San Francisco shields associated with Eburnean/Trans Amazonian orogeny (~2100–2050 Ma).

Keywords: Archean protoliths, colliding Congo-San Francisco shields, Eburnean/Trans-Amazonian orogeny, Transpression flow, Nyong Complex, SW Cameroon
Received: 10 March 2020; accepted: 31 August 2020; handling editor: M. Svojtka

1. Introduction

The SW Cameroon basement in Central Africa as part of the West Gondwana consists of the Ntem complex (NC), the Nyong complex (NyC) and the Oubanguide complex (OC) (Figs 1a, b) (Castaing et al. 1994; Trompette 1994; de Wit et al. 2008; Owona et al. 2011). The NC corresponds to the Archean NW Congo shield lithostructural unit. The NyC is the Cameroonian Paleoproterozoic unit as part of the West Central African fold belt (WCAFB) that recorded the Eburnean orogeny emplaced during the collision between the Congo and Sao Francisco shields (Fig. 1b) (Feybesse et al. 1998; Pénaye et al. 2004; Neves et al. 2006; de Wit et al. 2008). The OC, also named North Equatorial Fold Belt (NEFB), corresponds to the Neoproterozoic lithostructural unit. It consists of Precambrian to Neoproterozoic sediments reworked during the Pan-African orogeny associated with the collision between the Congo, West African and the Saharan shields (Fig. 1b) (Nzenti et al. 1988; Abdelsalam et al. 2002; Oliveira et al. 2006; de Wit et al. 2008; Saha-Foutsa et al. 2019). The crystalline basement is covered by the Cretaceous to Cenozoic Douala-Kribi-Campo sedimentary basin (Fig. 1b) (Maurizot et al. 1986; Tamfu et al. 1995; Oba 2001). Crystalline rocks have been abundantly explored by petrographical, geochemical, and geochronological studies conducting various models still under discussion. The NyC herein studied and, particularly, its geodynamic models, suffer from the lack of structural studies necessary for their consolidation.

However, such Proterozoic terranes offer possibilities to document the tectonic style associated with crustal growth-reworking during the Eburnean/Trans Amazonian orogeny in comparison with Archean and Phanerozoic terranes as well as vertical and horizontal plate tectonics. Various working hypotheses have been proposed regarding comparisons between Archean and Phanerozoic tectonic styles or between vertical and horizontal plate tectonics associated with crustal growth-reworking. For instance, Hamilton (2011) has demonstrated that Archean, Paleoproterozoic, and Mesoproterozoic rocks and structures differ significantly both from each other and from modern ones. Archean continental crust dominantly tonalite–trondhjemite–granodiorite (TTG), derived mostly by partial melting of protocrust and also from melting of both the subducted oceanic crust (Hamilton 2011) and from the base of thick basaltic plateaux formed above mantle upwellings (Bédard 2006). Contrarily, Paleopro-

terozoic and Mesoproterozoic orogens are largely ensialic. They derived from very thick basin-filling sedimentary and volcanic rocks on thinned Archean or Paleoproterozoic crust and remaining mafic protocrust (Vanderhaeghe et al. 1998; Hamilton 2011). These Proterozoic orogens supposed convergence, collision, and crustal thickening, similar to modern orogens (Vanderhaeghe et al. 1998).

Subduction zones display various horizontal contraction styles subjected to continental crust linked to convergent settings (Pfiffner 2006). They include thin-skinned tectonics that encompasses fold-and-thrust belts such as in the Cordilleran in southern Canadian Rocky Mountains, tectonically prograded over the margin of the continental Shields (Price 1981; Pfiffner 2006). They also comprise thick-skinned tectonics in which thrust faults cut across the entire upper crust and possibly the lower crust (Pfiffner 2006). They correspond either to crustal orogenic wedges or to orogenic plateaus but also a gravitational collapse of previously thickened crust, leading to the opening of intermontane and eventually oceanic back-arc associated with subduction zones (Vanderhaeghe 2012). They are also characterized by paired and unpaired metamorphic belts, the low-pressure metamorphic type formed beneath a volcanic chain in the adjacent island arc or continental margin, and the high-pressure metamorphic one, formed beneath a trench zone (Ernst 1973; Miyashiro 1973).

Baratoux et al. (2011) have documented Paleoproterozoic terranes bordering the West African Shield, a crustal thickening due to lateral shortening of volcanic island arcs and concomitant diapiric magmatic inputs associated with compressional regime later overprinted by transpression and thrust fault tectonics. Feybesse et al. (1998) proposed a first solid overview of the WCAFB and that of the NyC geodynamic evolution further corroborated by structural studies (Pénaye et al. 2004). Loose and Schenk (2018) and Houketchang Bouyo et al. (2019) have recently documented this evolution by characterizing eclogite metamorphism on MORB rock types emplaced in a subducted environment in addition to the granulite metamorphism previously established on Eseka paragneisses by Nédélec et al. (1993). Moreover, Toteu et al. (1994), Lerouge et al. (2006), Owona (2008), Loose and Schenk (2018), using various U–Pb zircon as Pb/Pb zircon techniques have established its Archean origin (>2700 Ma). The above authors also agreed that NyC corresponds to the NW Congo shield remobilized and emplaced during the Eburnean/Transamazonian orogeny between ~2400–1800 Ma associated with the collision between the Congo and Sao Francisco shields. Nédélec et al. (1993), Tchameni et al. (2001), and Shang et al. (2004) have established that the NyC derived from the partial melting of Archean protoliths using significant and rare-earth element contents and Sm/Nd isotopic signature showing Archean model ages ~3000 Ma. The NyC was affected by a polyphase deformation induced by a tectonic nappe transported top to the East onto the Congo shield (Feybesse et al. 1998; Pénaye et al. 2004; Owona et al. 2011). Details of the NyC tectonic evolution remain poorly known.

Indeed, the evolution of such orogenies includes classical subduction-collision events characterized by high P–T metamorphisms, tectonic imprints recorded both by sediments during their burial-exhumation and by pre- to orogenic granitoids. Those crustal deformations represent the key-criteria for characterization of orogenic belts. As natural laboratories, ancient terranes helped to answer some fundamental questions about the modes of crustal growth and lithospheric deformation through time (Sanderson and Marchini 1984; Tikoff and Teyssier 1994; Choukroune et al. 1995; Tikoff and Fossen 1995; Chardon and Jajananda 2008; Chardon et al. 2009; Gapais et al. 2009; Mvondo et al. 2017; Nakapelyukh et al. 2018). Such terranes display many deep-seated rocks exhumed from various depths inducing fold-and-thrust belts between colliding continental blocks (Price 1981; Pfiffner 2006; Omori et al. 2016; Kooijman et al. 2017). The Paleoproterozoic NyC appears as an excellent example of an old terrane between colliding Congo and Sao Francisco shields. It can thus serve to discuss the Eburnean/Transamazonian orogeny tectonic style.

Herein we provide new (i) petrography data on the Ngomedzap–Akongo area in the eastern part of the NyC; (ii) structure data with its steep tectonic features of a D_1–D_3 deformation including D_1–D_2 ductile phases, D_3 ductile-brittle and D_4 likely a late to post-orogenic brittle segment; and (iii) $^{207}Pb/^{206}Pb$ zircon ages of metagranodiorite and metasyenites that evidence the Archean origin of their protoliths and the NyC.

2. Tectonic setting

The NyC geodynamic evolution has started with the opening of earliest Archean sedimentary basins such as the Ogooué, Nyong, Ikobe–Waka and includes plutonic rocks dated between 2515–2435 Ma (Feybesse et al. 1998). These sedimentary and plutonic rocks were remobilized during the Eburnean/Trans Amazonian orogeny associated with the collision between the Congo and São Francisco Shields (Fig. 1b) (e.g., Feybesse et al. 1998; Neves et al. 2006; de Wit et al. 2008). Nevertheless, suture zones remain undiscovered.

NyC includes the Kama, Akongo and Govayang groups. The Kama group consists of TTG, meta-anorthoclasite, metagabbro, charnockite, gneiss, migmatite and amphibolite (Fig. 2). The Akongo group comprises banded iron formations (BIF), amphibolite, garnetite,

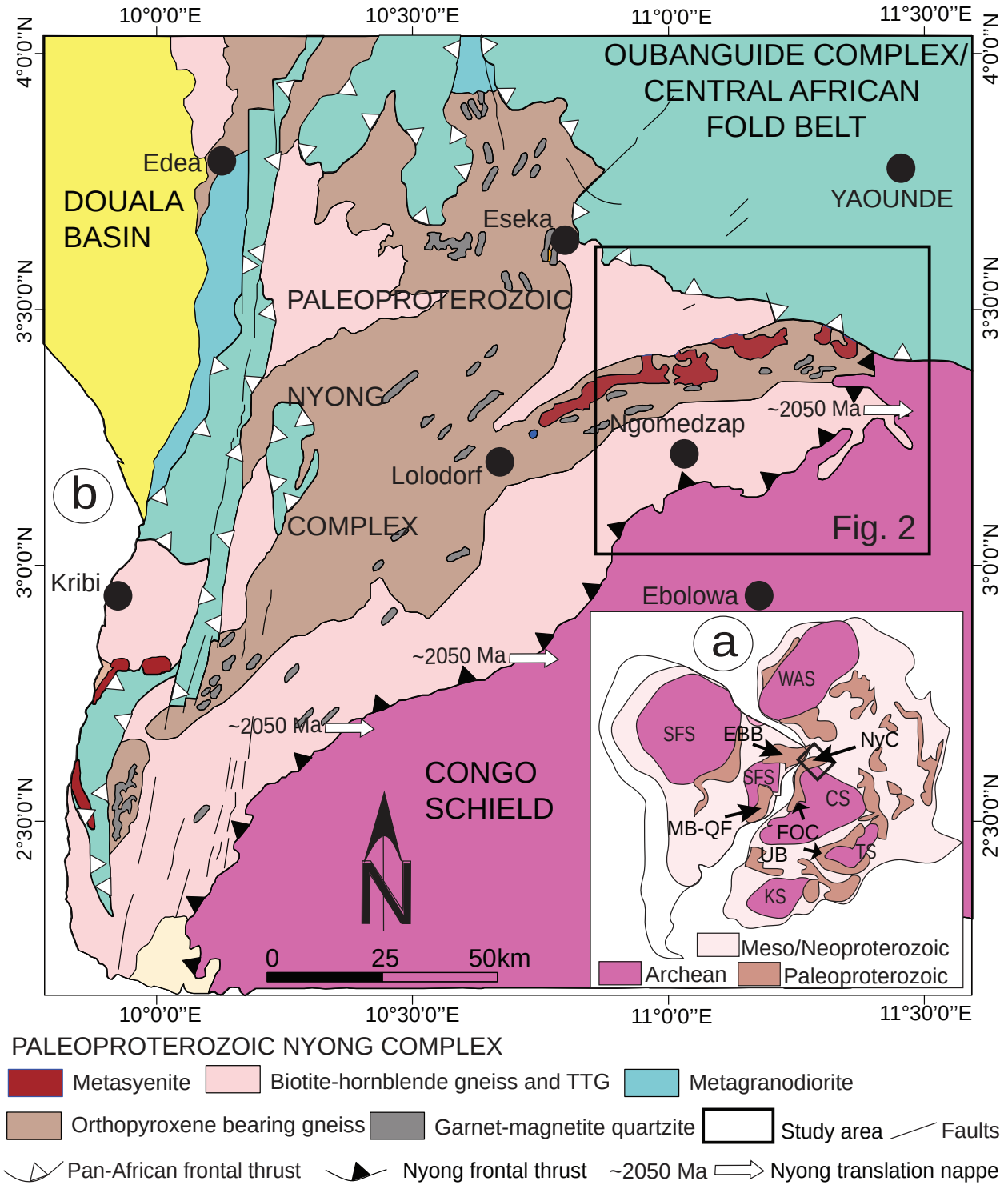

Fig. 1 a – South America–Africa fit showing shields and Proterozoic provinces of western Gondwana (modified after Castaing et al. 1994; de Wit et al. 2008; Lerouge et al. 2006; Neves et al. 2006; Owona et al. 2013) – CS: Congo shield, WAS: West African shield, TS: Tanzania shield, KS: Kalahari shield, SFS: Sao Francisco shield, AS: Amazonian shield, UB: Ubende belt, EEB: Eastern Bahia belt, MR–QU: Mineiro Belt-Quadrilátero Ferrifero, BM: Bumu complex. **b** – South-West Cameroon geological sketch showing its main lithostructural units, the Ngomedzap–Akongo area and sample locations used for geochronology.

eclogite, and alkali metasyenites. The Govayang group contains gneiss, BIF, amphibolite, and metagranitoids. Ledru et al. (1994), Feybesse et al. (1998), and Pénaye et al. (2004) defined three tectonic events affecting the

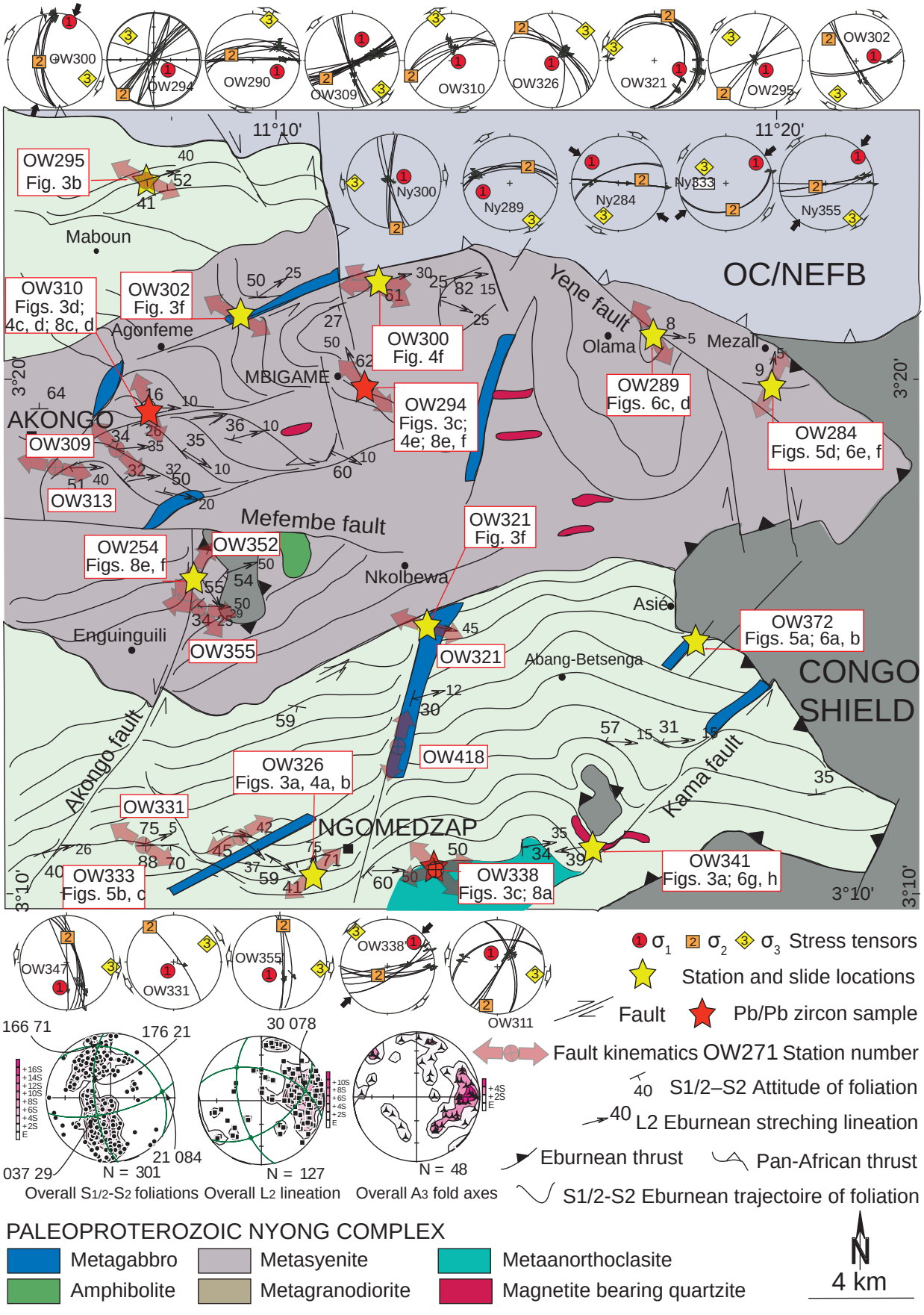
OW300
OW294
OW290
OW309
OW310
OW326
OW321
OW295
OW302
11°10'
11°20'
OW295
Fig. 3b
Maboun
Ny300
Ny289
Ny284
Ny333
Ny355
OC/NEFB
OW310
Figs. 3d;
4c, d; 8c, d
OW302
Fig. 3f
Agonfeme
OW300
Fig. 4f
Yene fault
Olama
Mezali
OW289
Figs. 6c, d
3°20'
MBIGAME
AKONGO
OW294
Figs. 3c;
4e; 8e, f
OW284
Figs. 5d; 6e, f
OW309
OW313
Mefembe fault
OW321
Fig. 3f
OW254
Figs. 8e, f
OW352
Nkolbewa
Asié
OW372
Figs. 5a; 6a, b
Enguinguili
OW355
OW321
Abang-Betsenga
CONGO
SHIELD
Akongo fault
OW326
Figs. 3a, 4a, b
OW418
Kama fault
OW331
NGOMEDZAP
OW333
Figs. 5b, c
OW338
Figs. 3c; 8a
OW341
Figs. 3a; 6g, h
3°10'
OW347
OW331
OW355
OW338
OW311
166 71
176 21
30 078
037 29
21 084
N = 301
N = 127
N = 48
Overall S1/2-S2 foliations
Overall L2 lineation
Overall A3 fold axes
σ1 σ2 σ3 Stress tensors
Station and slide locations
Fault
Pb/Pb zircon sample
Fault kinematics OW271 Station number
40 S1/2–S2 Attitude of foliation
40 L2 Eburnean streching lineation
Eburnean thrust
Pan-African thrust
S1/2-S2 Eburnean trajectoire of foliation
PALEOPROTEROZOIC NYONG COMPLEX
Metagabbro
Metasyenite
Metaanorthoclasite
Amphibolite
Metagranodiorite
Magnetite bearing quartzite
N
4 km

NyC and marked by the emplacement of the Nyong nappe transported top-to the East onto the Congo Shield. This nappe is dissected by C_3 sinistral blastomynolitic shear-zones (Owona et al. 2013). The brittle phase, represented by ~SW–NE faults, was associated with reactivations during the Pan-African orogeny (Pénaye et al. 2004).

The Eburnean metamorphism began early in Gabon where it peaked at *ca*. 2100 Ma (U/Pb zircon; Caen-Vachette 1988), under granulite to amphibolite conditions between 600–700 °C, 6–10 kbar in Ayem metapelites (Bonhomme et al. 1982; Ledru et al. 1994; Feybesse et al. 1998), and 650 °C, 7.5 kbar in Ndjole-Nkan-Nkolissen amphibolites (Feybesse et al. 1998). The NyC metamorphism in SW Cameroon encompassed at *ca*. 2050 Ma (U/Pb Zircon; Toteu et al. 1994), the amphibolite to granulite conditions 530–750 °C, 4–9 kbar in the Eseka migmatite and metapelites (Nédélec et al. 1993). However, Boniface et al. (2012), Loose and Schenk (2018) and Houketchang Bouyo et al. (2019) have recently described an old eclogite facies 800 °C, 16 kbar and 850 °C, 25 kbar, within the Eburnean-Transamazonian orogeny of southern Cameroon peaking at 2093 ± 45 Ma (U/Pb Zircon).

As Archean klippes encountered within the NyC (Fig. 2), the geochemistry supports field observations of the derivation of NyC rock types from the partial melting of the Archean crust (Nédélec et al. 1993; Toteu et al. 1994; Tchameni et al. 2001). The Sm and Nd isotopic characteristics established this Archean origin of most protoliths TDM ages at *ca*. 3000 Ma, (Tchameni et al. 2001). According to Vicat and Pouclet (1995) and Vicat et al. (1996), this complex was intruded by two dolerite magmatic phases. The first one with the back-arc basin tholeiitic and greenstone-belt volcanic character, which occurred between 2628 ± 33 Ma (Rb/Sr, WR) and 2347 ± 210 Ma (Sm/Nd, WR; Tchameni et al. 2001). Vicat et al. (1996) related them to the pre-Eburnean extensional magmatism (Vicat et al. 1996). The second phase, still undated, with typical continental tholeiite character, is linked to the pre-Pan-African extension (Vicat and Pouclet 1995; Vicat et al. 1996, 1997). Similar dolerites are mentioned in the Chaillu complex in Gabon as well as in Comba and Sembe Ouesso in the Republic of Congo and Lobaye valley in the Central African Republic (Feybesse et al. 1998). Boniface et al. (2012), Loose and Schenk (2018), and Houketchang Bouyo et al. (2019) defined within the NyC, with MORB-like eclogites that represent the subducted oceanic crust.

⇦

Fig. 2 The Ngomedzap–Akongo geological sketches showing mean of $S_{0/1/2}$ and S_2 foliations, L_2 stretching and mineral lineations, shear zones and faults treated with Speristat (lower hemisphere equal-area projections), location of outcrops and thin sections. **a** – note the regional folding drawn by the $S_{0/1/2}$ and S_2 foliations. **b –** the overall eastward strike and plunge dominantly parallel to L_2 lineations as A_2 fold axes of F_2 folds suggesting the D_2 continuous deformation, highlighting the transport top to the East of the NyC onto the Congo shield. **c –** multiple trends and kinematic sense of various faults evidencing their anachronous emplacement.

3. Samples and analytical methods

3.1. Petrography

We use classical lithopetrographical description from field observations in outcrop, hand sample description until optical microscopy in thin section. This enables us to determine the type of rocks as well as their microstructure, mineral composition, and mineral parageneses used for the deduction of metamorphic facies.

We also applied microtectonic technics in standard thin sections oriented as possible parallel to XZ sections of finite strain ellipsoid (normal to the foliation and parallel to the stretching lineation) to analyze fabrics that record ductile deformation and to identify pre-, syn- and post-tectonometamorphic mineral assemblages in respect of techniques proposed by Passchier and Trouw (2005). These fabrics were typified in the field and thin sections following classical methods (William et al. 1994; Tikoff and Fossen 1995; Passchier and Trouw 2005). We also analyzed blasts to link microstructures to deformation phases and to determine dynamic recrystallization features according to Kurse et al. (2001), Stipp et al. (2002), Passchier and Trouw (2005) and Owona et al. (2013).

3.2. Structural analysis

For the structural analysis, we identified and measured foliation (Sn), lineation (Ln), S–C foliation shear-fabrics, and faults on available outcrops for their geometry. Structural data were treated with Spheristat commercial program for the lower hemisphere and equal area, discriminating stretching (Str) and hornblende (Hbl) lineations. Faults were treated with both Spheristat and FS–Excel program for plotting great circles and fault striae as calculating orientations of principal stress axes (e.g., Angelier 1994) for fault arrays with the computer-program package of Sperner and Ratschbacher (1994). We refer to Appendix B of Ratschbacher et al. (2003) for details.

Kinematic or shear criteria such as S–C fabrics, offset markers, rotated porphyroclasts or porphyroblasts were studied to estimate the sense of ductile flow comprises shear-zones. For confirmation, we plot the dip of the Sn foliation, the plunge, and the pitch of L_2 stretching lineation in the ternary diagram of Chardon et al. (2009) modified after Balé and Brun (1989) for discussing the mode of crustal deformation.

3.3. Pb/Pb zircon geochronology

The zircon for $^{207}Pb/^{206}Pb$ single-grain geochronology were separated using the conventional procedure (Fig. 2) (crushing, Wilfley table, Frantz magnetic separator, heavy liquids, final handpicking). Single zircons from Ngomedzap metagranodiorite (Ow_{338}), Akongo (Ow_{310}), and Mbigame (Ow_{294}) metasyenite samples were analyzed at the Isotopenlabor, Technische Universität Bergakademie Freiberg in Germany. The method involves the deposition of Pb and other elements on a second filament, and subsequent measurement of Pb isotope ratios in a mass-spectrometer (Kober 1987). Before zircon evaporation, the second (ionization) filament was heated to 1800 °C to strip the filament from possible lead-bearing phases (additional outgassing). The evaporation filament was then heated to 1450 °C to remove common lead hosted in less stable phases of the zircon grain. Evaporation was performed at 1600 °C after cooling the ionization filament. This was done in one step to obtain high signal intensities for measurement. Data acquisition was performed by peak switching using a secondary electron multiplier equipped with an ion counter with mass sequence 207–206–204–206–207 (counting time in seconds 4–4–8–4–4, respectively). Each scan results in two $^{207}Pb/^{206}Pb$ and $^{204}Pb/^{206}Pb$ ratios. Five blocks (composed of ten scans) were recorded corresponding to 90 scans per measurement. Since $^{204}Pb/^{206}Pb$ ratios bear a large uncertainty due to the low intensity of ^{204}Pb, a trend line was defined through subsequently measured $^{204}Pb/^{206}Pb$ ratios. Each measured $^{207}Pb/^{206}Pb$ ratio was corrected with the according to $^{204}Pb/^{206}Pb$ ratio calculated from the trend line of the corresponding scan applying the Pb evolution model of Stacey and Kramers (1975). The obtained $^{207}Pb^*/^{206}Pb^*$ were corrected for mass bias (0.0036 per amu) deduced from NBS 981 and two zircon standards (zircon 91500 reported in Wiedenbeck et al. 1995, and zircon S–2–87, Wenham Monzonite, US Geological Survey). The calculated $^{207}Pb/^{206}Pb$ age of one zircon measurement and its 2σ mean error is based on the mean of all measured scans (usually 90) of isotope ratios with those omitted lying outside the 95% confidence level. The 2σ mean error of each measurement was increased by 5 Ma, corresponding to the uncertainty of the applied mass bias (±0.0022) determined by repeated measurements of standard zircons by different people over several years. During the course of measurement, the obtained $^{207}Pb/^{206}Pb$ ages of standard zircon 91500 (accepted value: 1065.4 ± 0.4 Ma) and S–2–87 (accepted value: 381.5 ± 4 Ma) yield 1064.9 ± 2.1 Ma (2σ mean, n = 13) and 379.7 ± 1.6 Ma (2σ mean, n = 44), respectively. As regards the dating of the evaporation technique, the mean age of several zircons from a sample was determined using the program ISOPLOT/EX 3.1 method (Ludwig 2001) to derive the mean weighted at the 95% confidence level.

4. Results

4.1. Petrography

The Ngomedzap–Akongo area consists of magnetite bearing quartzites, metagranodiorites, metaanorthoclasites, metagabbros, and metasyenites (Fig. 2). Archean charnockite occurs as Ntem Complex windows. The following lines present their petrography and discuss their evolution.

4.1.1. Magnetite-bearing quartzites

Magnetite-bearing quartzites (OW_{341}) correspond to banded iron formations described in the literature. They are red, foliated, and composed mainly of quartz in hand sample. They consist of quartz (50–55 %), magnetite (55–50 %), muscovite and zircon and display a granoblastic microstructure (Fig. 3a). Quartz shows hypidio- to idiomorphic coarse to stretched blasts (1–3 mm), chessboard polycrystalline fabric with undulose and patchy extinctions with inclusions of zircons. Quartz and muscovite lengthened flakes (1–2 mm) define felsic layers of the $S_{0/1/2}$ foliation. Magnetite (0.5–2 mm) forms stretched and isolated, as well as aggregate blasts parallel to the quartz layers and defines a L_2 mineral lineation.

4.1.2. Metagranodiorites

Metagranodiorites are pale green and foliated with felsic and mafic layers observable from outcrops to hand sample scales. They consist of plagioclase (50–55 %), quartz (20–25 %), microcline (5–10 %), biotite (< 5 %) and green amphibole (< 5 %) for a granoblastic microstructure. Oxide, diopside, apatite, and zircon are accessories, while sericite, epidote, and calcite are secondary (Fig. 3b). Plagioclase ($An_{20–40}$) shows subhedral to euhedral and antiperthitic grains (0.5–1 mm) with quartz, opaque, and zircon inclusions. They are transformed into epidote. Quartz forms polycrystalline ribbon and anhedral blasts (0.5–2 mm) with undulose and patchy extinctions. Flakes of biotite (0.5–1 mm) exhibit subhedral, kinked, rich in opaque. Perthititic microcline consists of recrystallized grains (0.5–1 mm) present in the matrix as the green amphibole, retromorphosed into epidote, and calcite in its inner zones and along its cracks. Opaques, apatite, calcite, and zircons (< 0.5 mm) occur as amoeboid to prismatic bordering green amphibole. They appear as euhedral-aligned microblasts in the matrix, inclusions in amphibole, and inclusions in biotites.

4.1.3. Metaanorthosites

Metaanorthosites (OW_{338}) are white-milky and foliated rocks, containing mainly feldspar. In thin section,

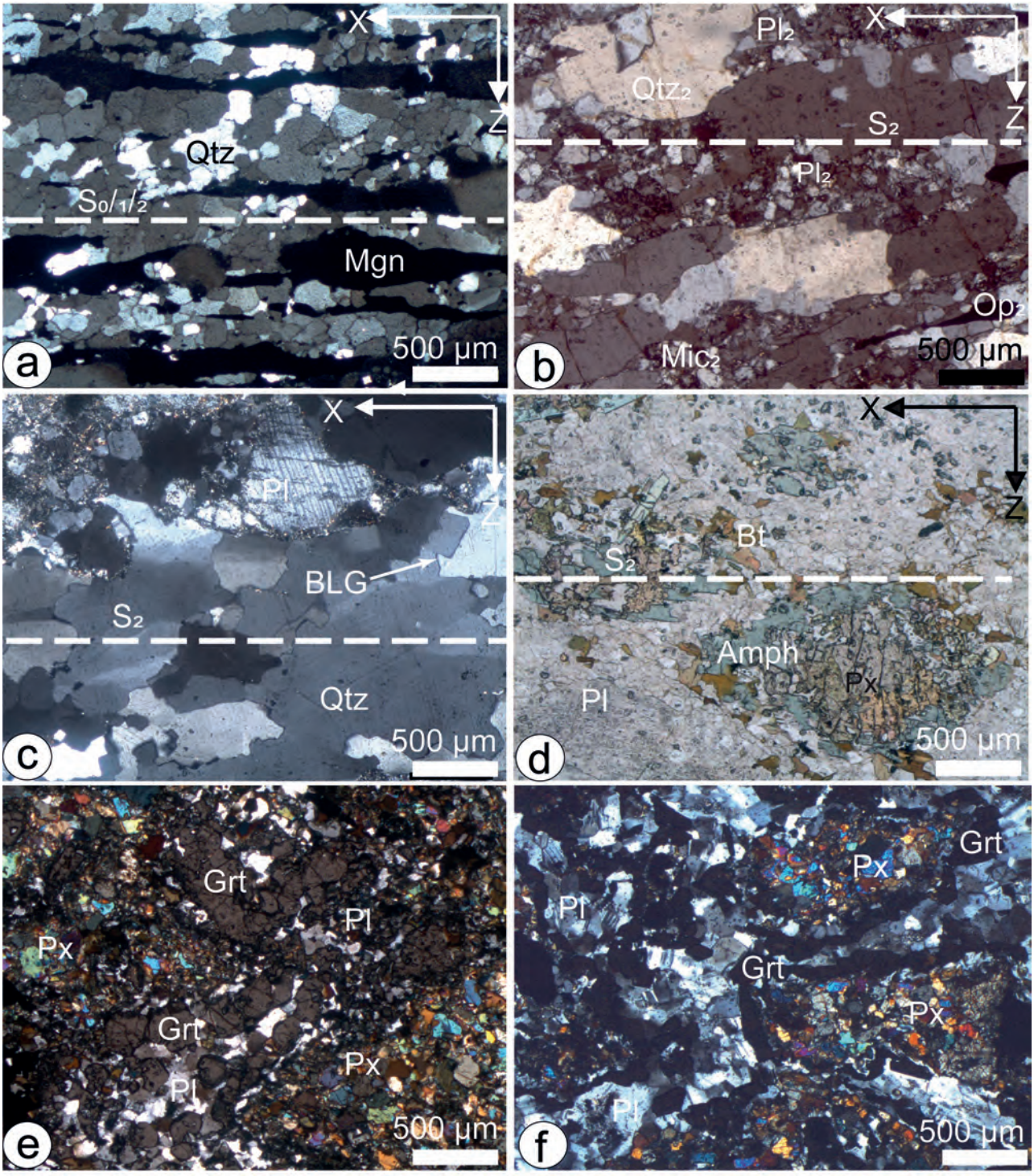

Fig. 3 The Ngomedzap–Akongo main granoblastic microstructures. **a –** quartz and magnetite layers outlining the $S_{0/1/2}$ foliation displayed by a granoblastic microstructure from Ngoulngal magnetite-bearing quartzite (sample OW_{341}; thin sections $PJ_{80–31, 32, 35}$). **b, c** – S_2 foliation in Akok metagranodiorites (thin sections $OW_{326, 354, 374}$; $PJ80_{12, 13, 17, 18}$) and Ngomedzap metaanorthosites (OW_{338}). **d** – S_2 foliation Mbigame mountain and Akongo metasyenites showing the uralitization of pyroxene ($OW_{294, 310}$). **e, f** – corona of garnet around plagioclase and clinopyroxene microstructure in metagabbros.

they contain plagioclase (75–80 %), quartz (5–10 %), diopside (5–10 %), green amphibole (< 2 %), apatite and zircon. Biotite, sericite, and epidote are secondary phases. They display a porphyro-granoblastic microstructure (Fig. 3c). Plagioclase ($An_{60–80}$) consists of hypidio- to idiomorphic grains (1–2 mm) with ver-

miculated antiperthite, deformed twins. It contains inclusions of quartz, opaque minerals and apatite. It is transformed into sericite and epidote. Quartz (0.2–2 mm) shows dynamically recrystallized grains with undulose and patchy extinction. Diopside (< 0.5 mm) consists of subhedral grains with opaque and quartz inclusions. Amphibole that derives from ouralization of diopside includes subhedral blasts (< 1 mm) bordered by oxides. Biotite develops along plagioclase microcracks. Apatite (< 0.5 mm) consists of idiomorphic grains. Zircons (< 0.5 mm) are idiomorphic grains in inclusions in plagioclases.

4.1.4. Metasyenites

Metasyenites (OW_{310}) are pink to pink-clear and massive rocks with amphibole and K-feldspar are recognizable in outcrops and hand samples (Fig. 3c). They display mainly of microcline (60–65 %), actinolite (20–25 %), augite (< 5 %), plagioclase (< 5 %) and quartz (< 5 %) that define a granoblastic microstructure (Figs 3c, d). Poikiloblasts of microcline include old magmatic cores surrounded by recrystallized rims, forming fine-grain fabrics in shear-zones and cracks. Green amphibole consists of magmatic grains (0.05–2 mm) and retromorphic blasts that derivate from the uralitization of augite magmatic old cores (0.02–0.1 mm; Fig. 3d). It is pseudomorphosed into calcite. Albites ($An_{0–5}$) and microcline contain old magmatic cores (0.05–5 mm) bordered by quartz and microcline microblasts. Biotites appear as idiomorphic inclusions (0.05–0.2 mm) in hornblende, the matrix and kinked blasts (0.2–0.5 mm). Apatite includes subhedral to euhedral grains (< 0.5 mm). Opaques show subhedral to euhedral grains (< 0.5 mm) in inclusion in green hornblende, pyroxene. Zircon occurs as inclusions in microcline and hornblende.

4.1.5. Metagabbros

Metagabbros (OW_{321}, OW_{372}) are dark and fractured rocks. They consists of plagioclase (40–45 %), augite (10–15 %), garnet (10–15 %), diopside (10–15 %), amphibole (5–10 %), opaque minerals (< 5 %), epidote, sericite and zircon that form a granoblastic to garnet corona microstructure (Figs 3e–f). Plagioclase ($An_{60–70}$) exhibits anhedral grains (0.5–1 mm) with deformed twinned crystals, opaque inclusions and transformation into epidote. Pyroxenes include augite and diopside idiomorphic cracked grains (0.2–0.8 mm), uralitized in subhedral to euhedral minerals amphibole (< 0.2 mm). Garnet (< 0.1 mm) shows idiomorphic blasts and the corona around pyroxene and plagioclase.

4.2. Structural analysis

4.2.1. Geometry

We discriminate two phases of ductile deformation, D_1–D_2, from the ductilobrittle D_3 and brittle D_4. D_1 corresponds to first increments of crustal thickening, represented by a sub-E–W $S_{0/1}$ foliation that results from transposition of S_0 (bedding) into a S_1, preserved as axial planes (S_1) of F_1 fold preserved in magnetite bearing quartzite, metagranodiorite, and metaanorthosite. Under the microscope, the $Qtz_1 + Mg_1 + Ms_1 + Zr_1$ in magnetite bearing quartzite (Fig. 3a; OW_{341}), $Qtz_1 + Pl_1 + Di1 + Mc_1 + Bt_1 \pm Op_1 \pm Zr_1$ in metagranodiorite (Fig. 3b, OW_{321}), $Pl_1 + Qtz_1 + Di_1 + Ap_1 \pm Op_1$ in meta-anorthosite (Fig. 3c; OW_{338}), and $Qtz_1 + Pl_1 + Di_1 + Mc_1 + Bt_1 \pm Ap_1 \pm Op_1$ in metasyenite (Fig. 3d; OW_{310}).

D_2 marked by sub-vertical structural features strongly overprints D_1 imprints (Fig. 4a). It transposed $S_{0/1}$, producing $S_{0/1/2}$ the dominant foliation in magnetite-bearing quartzites and S_2 foliation in metagranodiorites, meta-anorthosites, and metasyenites constituting metatexitic layering in their respective host rocks. $Qtz_2 + Mg_2 + Ms_2$ mineral assemblage defines the $S_{0/1/2}$ foliation in magnetite-bearing quartzites (Fig. 3a). S_2 mineral assemblages vary from type of rock to another. S_2 is represented by $Qtz_2 + Ser \pm Cal \pm Op_2 \pm Ep$ in metagranodiorites (Fig. 3b), $Qtz_2 + Pl_2 + Amp_2 \pm Op_2 \pm Bt_2$ in meta-anorthosites (Figs 3c, 4b) and $Qtz_2 + Pl_2 + Mc_2 + Hbl_2 + Bt_2 \pm Op_2$ in metasyenites (Figs 3d, 4c–f). L_2 lineation inferred to D_2, includes stretching and amphibole types. Both lineations are parallel and oriented WSW–ENE to WNW–ESE for an average strike N078°/30° (Fig. 2). They are parallel to A_2 axes (Fig. 2). This parallelism indicates the transport top to the East of the Nyong nappe onto the NC (Fig. 2). F_2 mesofolds are intrafolial with S_2 axial planes trending WSW–ENE to E–W, and parallel to the $S_{0/1/2}$ and S_2 foliations (Figs 2, 4a–d). They invariably affect meta-sediments and metaplutonites. These F_2 mesofolds are also isoclinal, dissymmetric to upright types suggesting a sub-horizontal shortening (Figs 4a, b).

The D_3 is represented by F_3 map-scale fold and C_3 shear-zones. The synthetic stereographic plot of the above foliations defines two main trends at N037°/29° and N166°/71° that suggest the existence of a regional F_3 fold oriented N176/21° (Fig. 2). C_3 SW–NE blastomylonitic shear-zones that dissect whole the NyC, are responsible S–C structures (Fig. 5). C_3 surfaces define an S_3 schistosity equivalent to high-strain features represented by $Qtz_3 + Pl_3 + Amph_3 \pm Mc_3 \pm Op_3 \pm Bt_3$ mineral assemblage that displays quartz, feldspar and amphibole dynamic recrystallizations as well as a S–C fabric (Fig. 5).

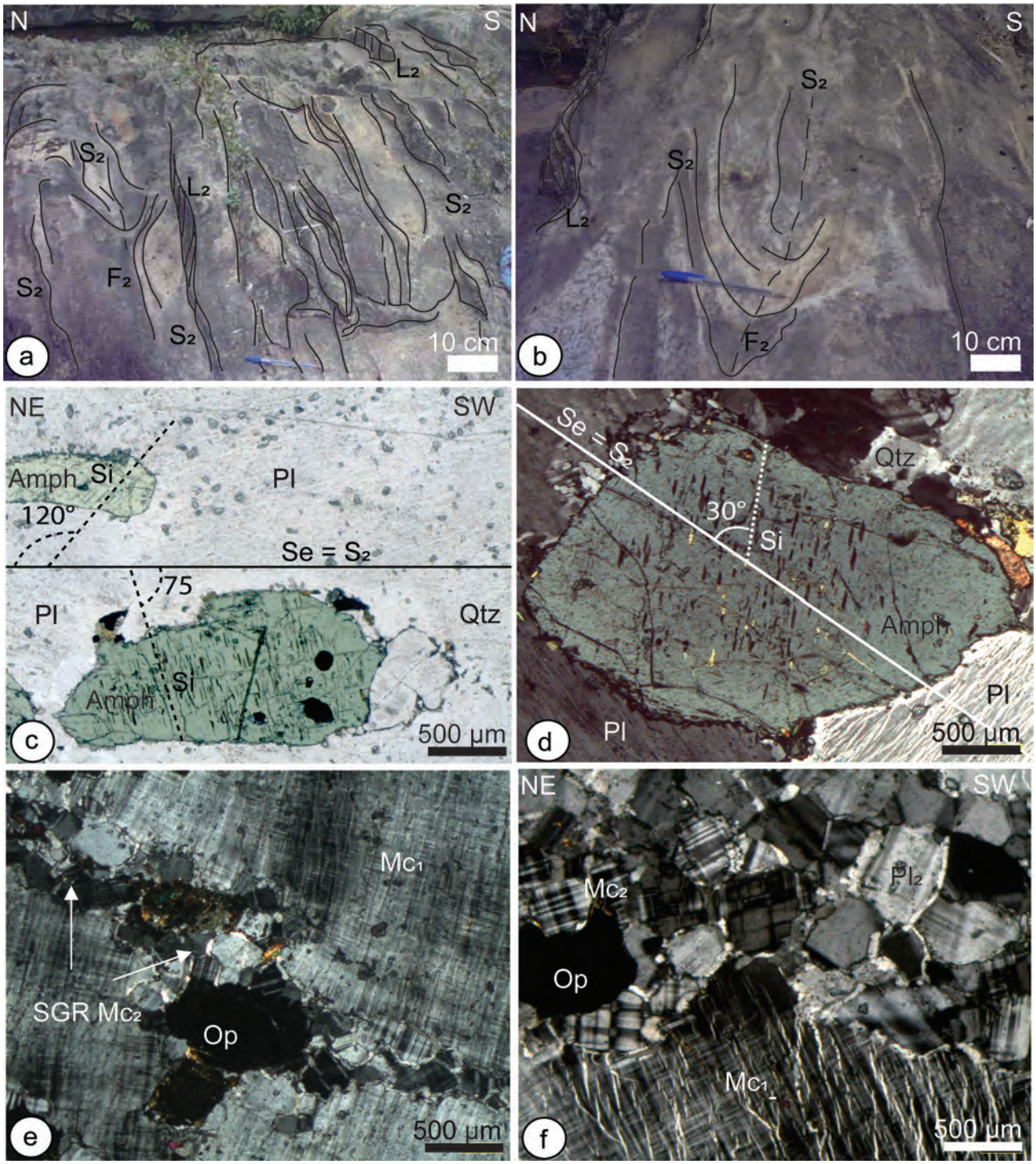

Fig. 4 The NyC S_n and S–C features. **a –** sub-vertical $S_{0/1/2}$ parallel to S_3 axial planes. **b, c** – S–C features in meta-anorthosites and metasyenites. **d, e** – intertectonic amphibole in Akongo metasyenites shown by various angles of 30°, 75° and 120° between Si equivalent of S_1 and similar to S_e (S_2 foliation) highlighting rotations recorded by amphibole minerals during their growth and suggesting the continuous character of the D_2–D_3 deformation. **f** – F_2 upright and intrafolial fold in Akok metaanorthosites with thinner flanks and thicker hinges suggesting the transport the Nyong nappe top to the East of the Congo shield under a transpression regime.

4.2.2. Kinematics

D_4 represents the brittle deformation. It shows NE–SW, NNE–SSW, ENE–WSW and E–W dip-slip, vertical strike-slip, dextro- and sinistro-normal faults, tension gashes, and tension fractures recorded from map- to microscopic scale (Figs 2, 6a–h). Tension gashes represent the last magmatic events. Tension fractures and inverse

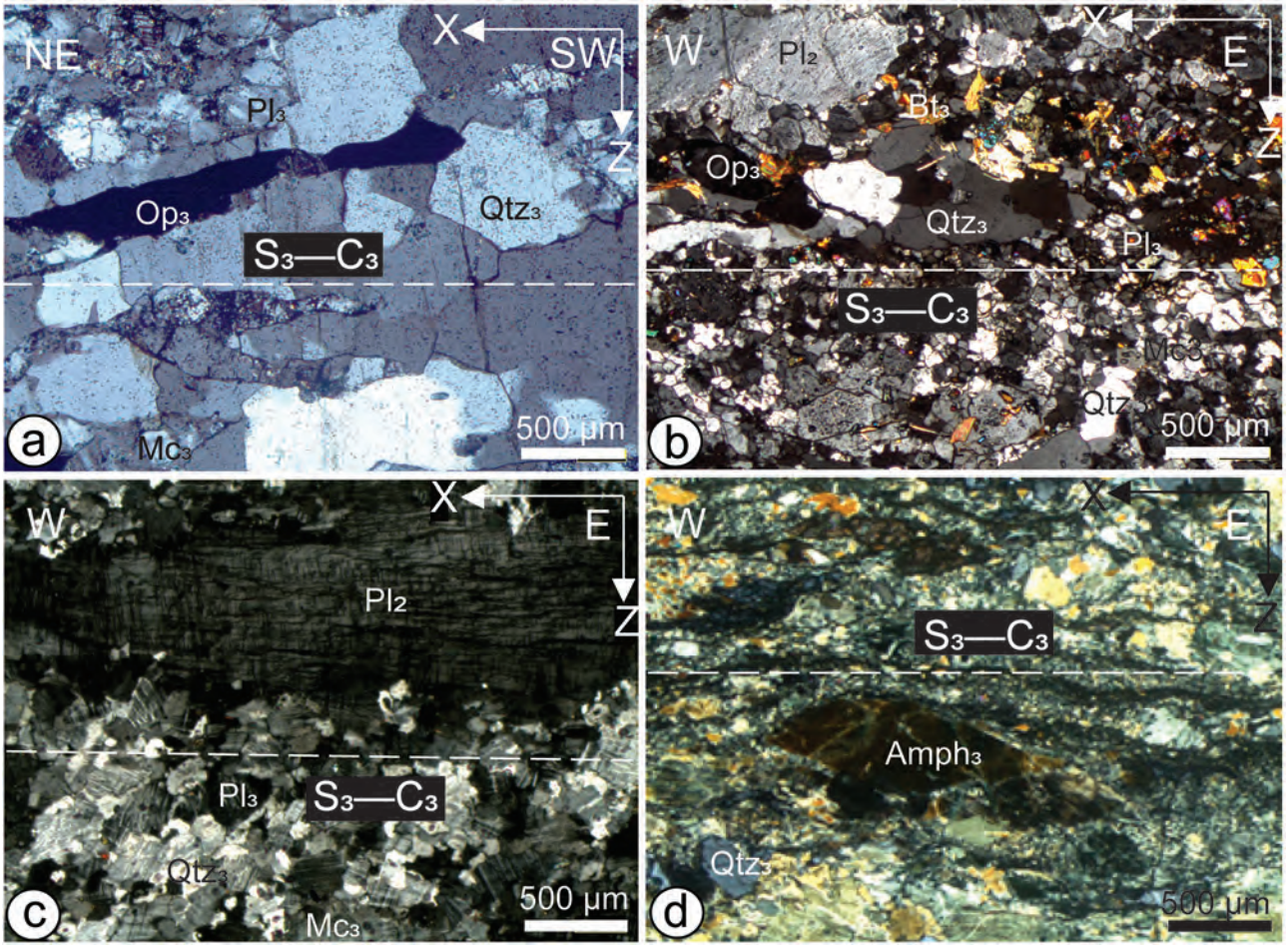

Fig. 5 Blastomynolitic shear zones in microscopic scale in the NyC. **a** – note a blastomynolitic shear zone underlined by the SGAR of quartz and SGR feldspars in the Enguingili metagranodiorites (OW_{354}). **b** – type-1 relict porphyroclast of microcline corroded by the SGR shape. **c** – the elongated ribbons quartz in a fine SGR mantle of microcline (OW_{292}). **d –** amphibole fish into a sinistral shear band in Olama metasyenites (OW_{284}).

dip-slip, vertical strike-slip, dextro- to sinistro-normal faults correspond to dry brittle tectonic features. The fault type, either reverse or normal faults, indicates a variation of shortening and extensional tectonic regime. The σ_1, σ_2 and σ_3 principal stress axes display these anachronous occurrences (Figs 2, 6a–h). The most dominant strain regime induced wrench fault types. The multiple nature of D_4 lithoclases shows that the NyC recorded various post-orogenic brittle tectonic phases.

We used the $S_{(n)}$ foliations, $L_{(n)}$ lineations, $F_{(n+1)}$ meso- to cartographic folds, inter-tectonic and S–C structures, offsets as the σ(n) principal stress axes of shear-zones and faults for highlighting the NyC kinematics. The perfect layering $S_{0/1/2}$ in magnetite bearing quartzites represented by the quartzite and magnetite parallel layers indicate the transposition of the S_0 bedding to the earliest $S_{0/1}$ foliation under a D_1 pure shear-regime or lateral flow fabric The occurrence of the sub-vertical S_1 foliation in metagranodiorites, meta-anorthosites and metasyenites indicates their syn-D_1 diapiric intrusion shown by sub-vertical magmatic fabric or vertical flow fabric associated with subduction zones.

The eastward and sub-horizontal nature of the transposed $S_{0/1/2}$ foliation in magnetite bearing quartzites specify the transport top to the East of the NyC onto the Congo shield associated with D_2 (Figs 1b, 2). The eastern plunging of the L_2 stretching and amphibole lineations in para- and orthoderived rocks (Fig. 2), as well as sub-vertical S_2 foliations in metagranodiorite, meta-anorthosite, and metasyenite with western vergences (Figs 2, 4b), corroborated the eastward transport of the Nyong nappe onto the Congo shield (Figs 2, 4a, b). This indicates the transpression nature of D_2 (Fig. 7).

⇨

Fig. 6 The NyC prototype macro- and microscopic brittle structures showing various types of lithoclases. **a, b** – sub-N–S strike-slip fault cross-cutting metasyenites on the Nyong River with men as scales. **c, d** – sub-N–S strike-slip fault cemented by quartzite injections and cross-cutting metasyenites with a pen and compass as scales. **e, f** – Dextra-normal fault cross-cutting the metagranodiorites on the Nyong River border. **g, h** – Sinistro-normal fault cross-cutting the magnetite--bearing quartzite.

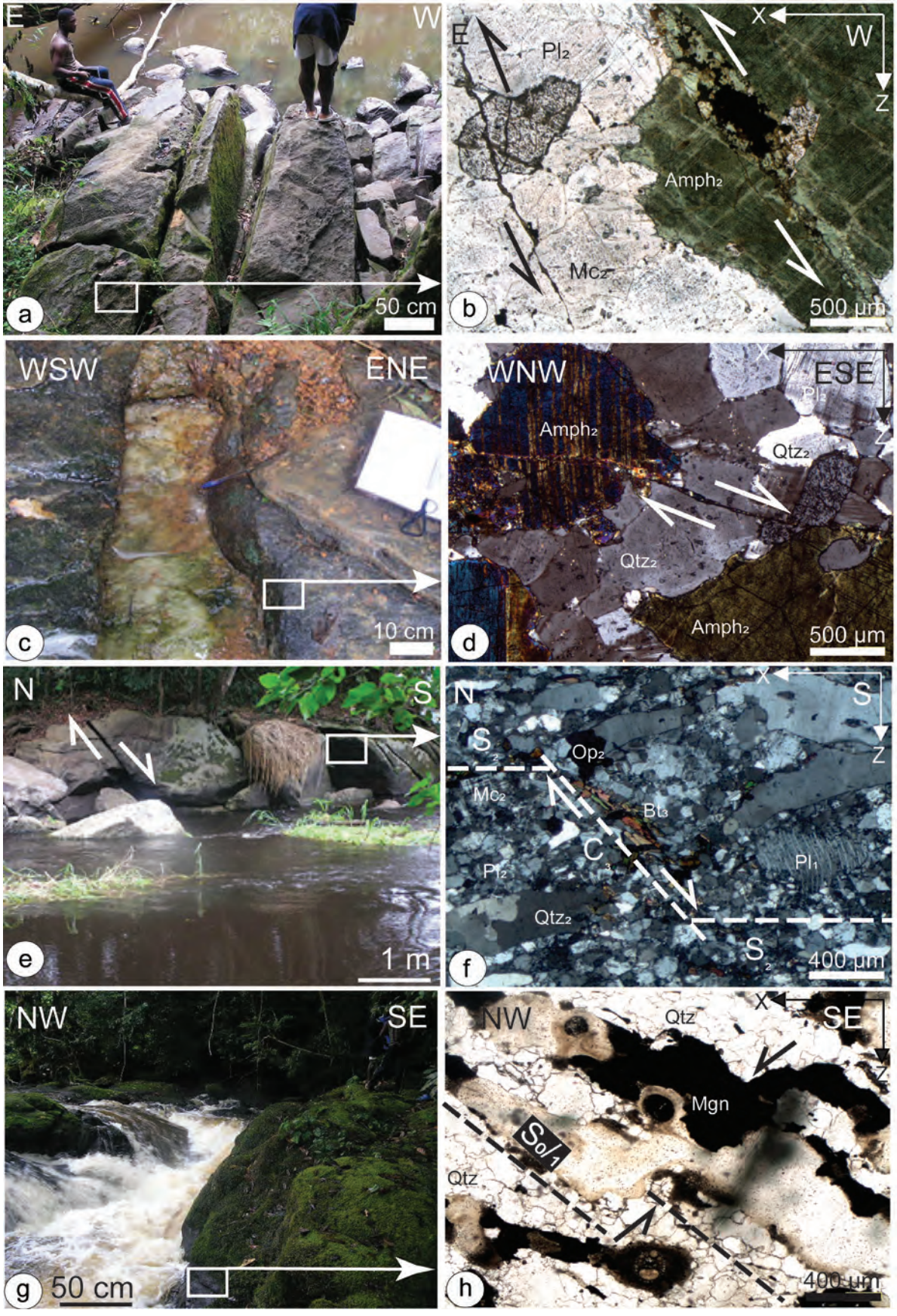
E
W
50 cm
a
X
W
Z
E
Pl2
Amph2
Mc2
500 µm
b
WSW
ENE
10 cm
c
WNW
ESE
Amph2
Qtz2
Qtz2
Amph2
500 µm
d
N
S
1 m
e
N
S
X
Z
S2
Op2
Mc2
Bt3
C3
Pl2
Pl1
Qtz2
S2
400 µm
f
NW
SE
50 cm
g
NW
Qtz
X
SE
Z
Mgn
Sol1
Qtz
400 µm
h

Eastward and westward ticker hinges of sub-vertical F_3 meso-folds support the continuum transpression tectonic regime for D_3 (Figs 4a, b). This is corroborated by the parallelism between $S_{0/1/2}$ and S_2 foliations with S_2 axial plane as well as inter tectonic minerals represented by various S_i–S_e features in metasyenite (Figs 4c, d). They highlight the ductile characters of the D_2 deformation. The amphibole inter-tectonic microstructures evidence the S_i rotational internal schistosities that may represent the earliest magmatic fabric that has been recorded during D_1 with the S_e external schistosity corresponding to S_2 foliation. The uralitization of pyroxene into amphibole that defined L_2 mineral indicates the D_2 deformation peaked under the amphibolite facies.

D_3 is materialized by S–C features as well as blastomylonitic shear-zones almost marked by dynamic recrystallized amphibole, feldspar and quartz blasts.

Tension gashes, tension fractures, and faults oriented NE–SW, NNE–SSW, ENE–WSW, and E–W, their associated offsets and respective σ_1, σ_2 and σ_3 principal stress axes, likely define the D_3 anachronous character (Figs 2, 6a–h). Tension gashes represent last magmatic events while tension fractures and inverse dip-slip, vertical strike-slip, dextro- to sinistro-normal faults correspond to dry brittle tectonic features and their complicated nature as the reverse and normal faults linkable to shortening and extensional tectonic regime, respectively. The existence of various σ_1, σ_2 and σ_3 principal stress axes indicate multiple reactivations (Fig. 2). The D_3 most dominant strain regime induced wrench fault types.

4.3. Pb/Pb zircon geochronology

We have obtained the $^{207}Pb/^{206}Pb$ zircon evaporation ages from samples Ow_{338}, Ow_{310} and $Ow_{294,}$ as shown in Tab. 1 and Fig. 8. Sample Ow_{338} from the Ngomedzap metagranodiorite shows short to long-prismatic (125–250 µm) (near-idiomorphic and yellow to pink zircons). Out of the seven grains measured, four gave the similar $^{207}Pb/^{206}Pb$ age with a mean value of 2760 ± 26 Ma (*MSWD* = 0.81) while the three other grains produced considerably older and younger $^{207}Pb/^{206}Pb$ ages at *ca*. 2817.5 ± 2.7 Ma, 2698.6 ± 2.8 Ma and 2672.7 ± 3.1 Ma. All suggest their Neoarchean origin (Figs 8a, b).

The Akongo metasyenite sample Ow_{310} displays short to long-prismatic, idiomorphic and yellow to pink zircons. From the eight grains measured, five provided a $^{207}Pb/^{206}Pb$ mean age of 2792 ± 13 Ma with *MSWD* = 1.3. Three further grains display considerably younger $^{207}Pb/^{206}Pb$ ages at ca. 2639.7 ± 3.2 Ma, 2573 ± 4.7 Ma and 2552.2 ± 3.2 Ma (Tab. 1; Figs 8c, d). They indicate their Neoarchean origin, too.

The sample Ow_{294} from the Mbigame metasyenite provided long, prismatic to subeuhedral and yellow to pink zircons. From the seven zircons analyzed, four gave the $^{207}Pb/^{206}Pb$ mean age of 2795 ± 3 Ma with *MSWD* = 0.28 and the $^{207}Pb/^{206}Pb$ relative younger ages on the three other grains at *ca*. 2741.8 ± 4.5 Ma, 2737.6 ± 2.6 and 2730.7 ± 1.4 Ma (Figs 8e, f). They equally evidence their Neoarchean origin.

The nine pooled data from both metasyenite samples yielded a mean age of 2785 ± 12 Ma with *MSWD* = 0.76. We preferred as the best mean age of 2789 ± 13 Ma with *MSWD* = 0.19 excluding single zircon,

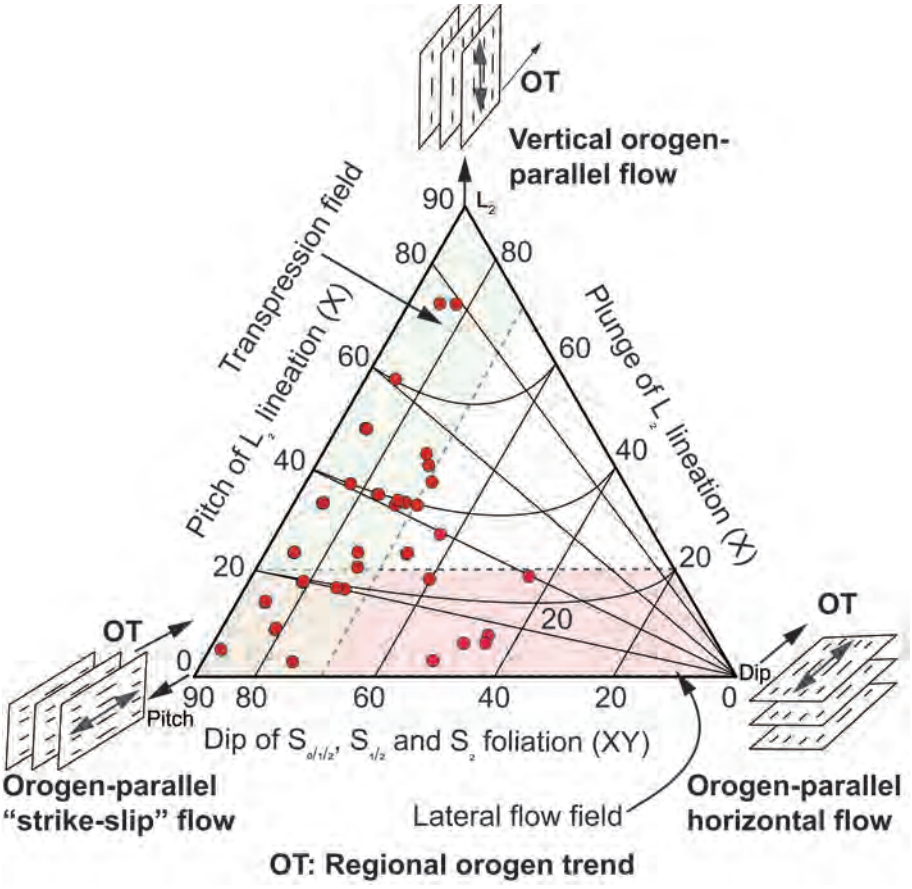

Fig. 7 NyC fabric data plotted in the crustal flow mode diagram of Chardon et al. (2009) (modified after Balé and Brun 1989). Note interference between transpression and horizontal flow fabrics pattern registered in NyC magnetite bearing quartzite, metagranitoids and metasyenites.

Tab. 1 $^{207}Pb/^{206}6Pb$ evaporation measurements of single zircon grains and calculated mean ages and GPS coordinates from metasyenites from Ngomedzap metagranodiorite (OW_{338}), Mbigame mountain (OW_{294}) and Akongo (OW_{310})

Sample		Grain	Mass scan	$^{204}Pb/^{206}Pb$	2σ	$^{207}Pb/^{206}Pb$	2σ	$^{207}Pb/^{206}Pb$ age	2σ
Ow338		Ow338Zr4	90	0.0003180	0.0000094	0.2019800	0.0003370	2817.50	2.70
		Ow338Zr2	60	0.0005540	0.0000270	0.1976500	0.0006610	2757.10	5.40
		Ow338Zr6	90	0.0001500	0.0000044	0.1946900	0.0003450	2772.90	3.10
		Ow338Z8	90	0.000Ow3380	0.0000057	0.1946700	0.0001370	2753.50	1.20
	Mean for four grains		330	0.0003400	0.0000116	0.1972475	0.0003700	2775.25	3.10
						Isoplot mean with total correction		2764 ± 28 Ma	
	Unconsidered grains in calculation	Ow338Z9	90	0.000529	0.0000127	0.1907500	0.0003110	2698.60	2.80
		Ow338Zr5	90	0.000689	0.0000136	0.1898500	0.0002780	2672.70	3.10
Ow294		Ow294Z9	90	0.000102	6.59E-06	0.1938	0.000388	2770.2	3.4
		Ow294Z4	60	0.000121	4.13E-06	0.1956	0.000241	2783.6	2
		Ow294Z1	27	0.0000747	0.0000136	0.19716	0.000982	2798.3	5.7
		Ow294Z8	90	0.0000804	2.86E-06	0.20072	0.000112	2830.2	0.9
	Mean for four grains		267	0.0000945	0.0000068	0.1968200	0,0004308	2795.58	3.00
						Isoplot mean with total correction		2816 ± 34 Ma	
	Unconsidered grains in calculation	Ow294Z2	90	0.000081	0.00000176	0.18896	0.000162	2730.7	1.4
		Ow294Z3	90	0.000078	0.0000121	0.19012	0.000544	2741.8	4.5
		Ow294Z10	90	0.0000063	0.00000324	0.18955	0.000309	2737.6	2.6
Ow310		Ow310Z7	89	0.0001370	0.0000020	0.1955100	0.0001030	2781.10	0.80
		Ow310Zr4	90	0.0000434	0.0000009	0.1957400	0.0001320	2792.50	1.10
		Ow310Zr6	88	0.0001660	0.0000063	0.1971100	0.0002810	2792.90	2.10
		Ow310Z8	90	0.0000892	0.0000024	0.1959700	0.0000926	2792.90	0.80
		Ow310Z11	90	0.0002410	0.0008640	0.1983000	0.0002930	2812.20	2.50
	Mean for five grains		447	0.0001353	0.0001751	0.1965260	0.0001597	2794.32	1.46
						Isoplot mean with total correction		2789 ± 13 Ma	
	Unconsidered grains in calculation	Ow310Zr5	90	0.000462	0.00000674	0.18357	0.000289	2639.70	3.20
		Ow310Zr8	90	0.000181	0.0000039	0.17323	0.0000442	2573.50	4.70
		Ow310Z9	90	0.00036	0.000000707	0.16945	0.000312	2552.20	3.10

the youngest one for the pooled-data from above metasyenite samples (Figs 8g–j). All the three analyzed samples provided mean age of 2793 ± 12 Ma with *MSWD* = 1.2, calculated as the mean of all fifteen single zircon age. We retained as the best mean age for the three samples, an identical to the mean above syenites and equal to 2789 ± 13 Ma with *MSWD* = 0.28, calculated from eleven data of the three analyzed samples, rejecting two, the youngest and oldest single zircon ages (Figs 8i–j). These two best mean ages are the same, quite close to individual sample ages and suggest their common Neoarchean origin. Given the spread in individual age data and analytical uncertainties, it is also possible that the three studied rocks are coeval, and their pooled age of *ca*. 2790 Ma is the best time estimate of their intrusion.

5. Discussion

Using the lithostructural and geochronological data, we discuss in this section how the Ngomedzap-Akongo area in the eastern part of the NyC has recorded the collision between the Congo and Sao Francisco shields as a continent-continent collision type during the Eburnean orogeny (Feybesse et al. 1998; Lopez et al. 2001; Lerouge et al. 2006; Neves et al. 2006; Aguilar et al. 2017).

The lithopetrography of the NyC displays magnetite bearing quartzite, metagranodiorite, metaanorthosite, metagabbro, and metasyenite (Figs 1b, 2). Such rocks usually encountered in collision orogenies, record classical plate tectonism during their burial uplift passage as in pre- to syntectonic granitoids defining the modes of lithospheric deformation and crustal growth through time (Choukroune et al. 1995; Chardon and Jajananda 2008; Chardon et al. 2009; Gapais et al. 2009; Hamilton 2011; Nakapelyukh et al. 2018). The NyC seems to obey similar tectonic evolution (Feybesse et al. 1998; Pénaye et al. 2004; Houketchang Bouyo et al. 2019; Loose and Schenk 2018). Baratoux et al. (2011) have documented a similar Paleoproterozoic crust evolution during the Eburnean orogeny around the West African Shield.

Blastic fabrics observed in studied rocks indicate their metamorphic character (Figs 3a–c). Quartz with undulose and patchy extinction (Figs 3a–c, 5a–c, 6d, f), relict feldspar with deformed twins and their dynamic recrystallized microblasts (Figs 3b, c, 4e, f, 5b, c) mark the D_2 ductile deformation. The corona microstructure of garnet separating plagioclase to clinopyroxene and amphibole highlights a decompression in NyC metagab-

bros due to their deepest origin, rapid uplift and cooling caused by exhumation (Loose and Schenk 2018; Houketchang Bouyo et al. 2019). This evolution is associated with the collision between the Congo and Sao Francisco shields and likewise be related to the eburnean/Trans Amazonian orogeny (Feybesse et al. 1998; Lopez et al. 2001; Lerouge et al. 2006; Neves et al. 2006; Aguilar et al. 2017). Passchier and Trouw (2005) related such microstructures to retrograde metamorphisms and cooling processes. Such metamorphic segment is documented in the NyC metabasites corresponding to MORB-like (Owona 2008; Boniface et al. 2012; Loose and Schenk 2018; Houketchang Bouyo et al. 2019). The above NyC lithological assemblages in terms of magmatic-tectonic context, including BIF, "MORB-like" rocks and felsic plutonic rocks, indicate the collisional continent-continent tectonic environment in Cameroon (Saha-Fouotsa et al. 2019).

Moreover, the NyC mineral associations and specific microstructures suggest two primary metamorphic schemes, the high-temperature and the high-pressure types of the Eburnean metamorphism. The uralitization of pyroxene into amphibole indicates the retrograde metamorphism marked by a drop of temperature, from that may range from the granulite to amphibolite facies. These mineral transformations are consistent with isobaric cooling segments. Nédélec et al. (1993) have documented such P–T segments with the garnet–plagioclase–biotite mineral association of the Eburnean metamorphism in Eseka paragneisses. The pyroxene-garnet-plagioclase mineral assemblage and their associated corona microstructure evidenced by overgrowths of plagioclase and clinopyroxene around garnet blasts indicate the brutal decrease of the pressure of our metagabbros. This corresponds to nearly isothermal decompression of the same Eburnean metamorphism. Loose and Schenk (2018) and

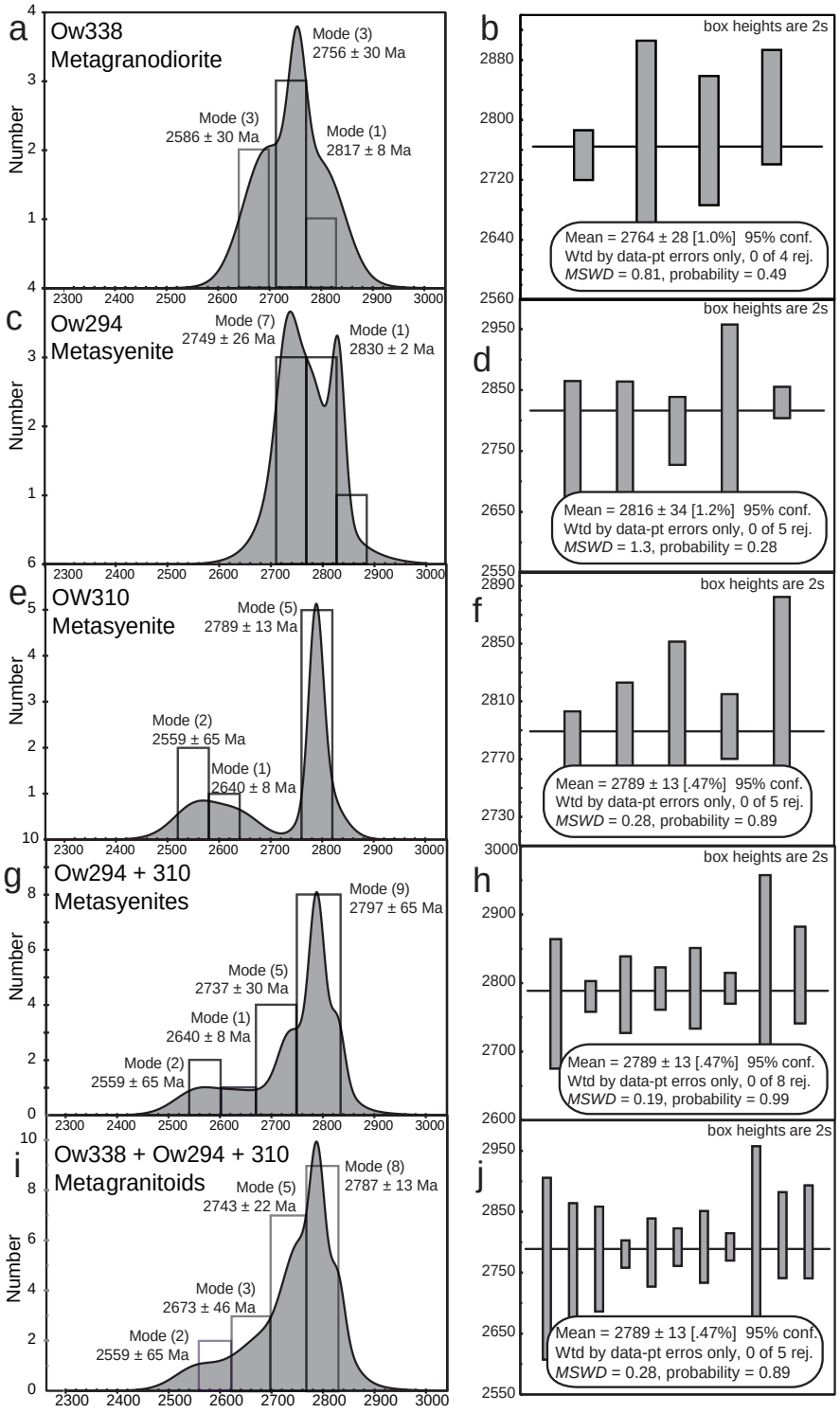

Fig. 8 Single zircon grain $^{207}Pb/^{206}Pb$ evaporation ages (shown as error bars for each measured zircon grain) and calculated weighted mean ages for the three analyzed samples of metagranodiorites and metasyenites. Note the various set of Archean ages that suggest their Archean origin and multiple reactivations.

Houketchang Bouyo et al. (2019) have described such microstructures with P–T paths dropping from the eclogite to the amphibolite facies. Ultimately, feldspar saussuritization and damouritisation into epidote and sericite, as well as the chloritization of biotite, highlight subsurface mineral transformations. They represent late cooling stages of the Eburnean metamorphism that drop until the greenschist facies (Owona 2008). These mineral parageneses display various stages of the Eburnean/Trans Amazonian metamorphism recorded by the NyC (Nédélec et al. 1993; Pénaye et al. 2004; Owona 2008; Loose and Schenk 2018; Houketchang Bouyo et al. 2019). They are consistent with low-pressure and high-pressure metamorphic belts usually associated with colliding settings (Ernst 1973; Miyashiro 1973). The occurrence of metasediment and metaplutonite rock types indicate that the NyC has recorded a crustal growth and thickening as continent-continent orogenies (Choukroune et al. 1995; Gapais et al. 2009). They highlight its geodynamic processes alike in plate tectonics where exhumed multiple deep-seated rocks from various depths have produced the NyC fold-and-thrust belts between colliding continental blocks (Price 1981; Pfiffner 2006; Omori et al. 2016; Kooijman et al. 2017), herein the Congo and Sao-Francisco shields, similar to modern orogens (Vanderhaeghe et al. 1998).

We used NyC tectonic imprints, $S_{(n)}$ surfaces, $L_{(n)}$ lineations, $F_{(n+1)}$ meso- to cartographic folds, inter-tectonic and S–C structures, offsets as the $\sigma_{(n)}$ principal stress axes of shear-zones and faults for discussing and evaluating geodynamic processes that exhumed NyC rocks and characterized its fold-and-thrust belts. Nédélec et al. (1993), Feybesse et al. (1998), and Pénaye et al. (2004) retained two ductile phases and a third one dedicated to the brittle deformation. Batroux et al. (2011) did the same in West African Paleoproterozoic belts. Our field observations, thin sections, and the stereographic treatment through tectonic imprints and mineral parageneses highlight a dominantly D_3 ductile-brittle phase. We interpret brittle features as post-orogenic in a single D_4 phase. The $S_{0/1}$ transposed foliation in magnetite bearing quartzites is typical of a D_1 pure shear-regime in pre-orogenic old basins. Such transpositions are described within the WCAFB, notably in the NyC of Cameroon and in its homologous, the Ogoué and Franceville complexes of Gabon. The nearly-sub-vertical S_1 in metagranitoids corresponds to magmatic fabric related to their diapiric occurring mode. The associated relict mineral parageneses $Mg_1 + Ms_1 + Zr_1 + Qtz_1$ in magnetite-bearing quartzite and $Pl_1 + Di_1 + Mc_1 + Qtz_1 \pm Amp \pm Bt_1 \pm Op_1 \pm Zr_1 \pm Ap_1$ in metagranodiorite, meta-anorthosite and metasyenite indicate that the D_1 operated under granulitic conditions (Figs 3a–d). Such fabrics are ubiquitous in convergent settings (Price 1981; Pfiffner 2006; Vanderhaeghe 2012).

The NyC displays mineral inter-tectonic and Si–Se rotational or internal microstructures (Figs 4c, d). They highlight the D_1 strongest overprinted by D_2. Poekiloblasts of D_2 that have incorporated inclusions of quartz, opaques, zircons that form Si equivalent to S_1 during their crystallization. D_2 mineral parageneses that include $Qtz_2 + Mg_2 + Ms_2$ and $Qtz_2 + Pl_2 + Mc_2 + Amph_2 \pm Bt_2$ represent the $S_{0/1/2}$ and S_2 foliations in magnetite bearing quartzites and metagranitoids, respectively. The ubiquitous presence of amphibole in the above metaplutonites indicates that D_2 operated under amphibolite conditions. This is reliable with Pénaye et al. (2004). The sub-vertical character of both $S_{0/1/2}$ and S_2 foliations, the F_2 upright and isoclinal mesofolds with sub-vertical and sub-E–W S_2 axial plane, sub-horizontal A_2 fold axes parallel to L_2 lineations plunging either to the East or to the West (Fig. 2), the thickest eastward or westward hinges and thinned flanks of these meso-fold types (Figs 4a, b) indicate that D_2 was dominantly a transpression tectonic regime or parallel orogen strike flow. This is consistent with the diagram of the tectonic model shown in Fig. 6 (Sanderson and Marchini 1984; Tikoff and Teyssier 1994; Chardon et al. 2009; Mvondo et al. 2017). Baratoux et al. (2011) described similar tectonic evolution marked by compressional regime later overprinted by transpression and thrust fault tectonics in the Eburnean orogeny in West Africa as well as Carreras and Druget (2018) and Fossen et al. (2018) when discussing the progressive or multiphase nature of orogenic deformations. The above features corroborate eastward transport of the Nyong nappe top to the East onto the Congo shied as established previously (Nédélec et al. 1993; Feybesse et al. 1998; Pénaye et al. 2004; Lerouge et al. 2006; Owona et al. 2011). It corresponds to the fold-and-thrust belts colliding between continental blocks, as demonstrated by Omori et al. (2016). Continental blocks herein concerned are the Congo and Sao Francisco shields (Feybesse et al. 1998; Lopez et al. 2001; Lerouge et al. 2006; Neves et al. 2006; Aguilar et al. 2017).

D_3 induced F_3 cartographic folds and S–C structures that affect $S_{0/1/2}$ and S_2. These megafolds displayed by the synthetic stereographic plot of the above foliations define two main trends at N037°/29° and N166°/71° and form lithostructural unit of the Nyong nappe (Fig. 2). Shear-zones are blastomylonitic C_3-type, oriented SW–NE and differentiated into proto-, meso- and ultra-mylonites (Fig. 5; Owona et al. 2013). They are responsible of S–C structures, dynamic recrystallization features, and the associated low- to high-strain anisotropies. The associated C_3 mineral parageneses made of $Qtz_3 + Pl_3 + Amph_3 \pm Mc_3 \pm Bt_3 \pm Op_3$. Owona et al. (2013) have described these shear-zones as a natural laboratory of crystal dynamic recrystallization, consistent with shear-zone microtectonics of Passchier and Trouw (2005), Stipp et al.

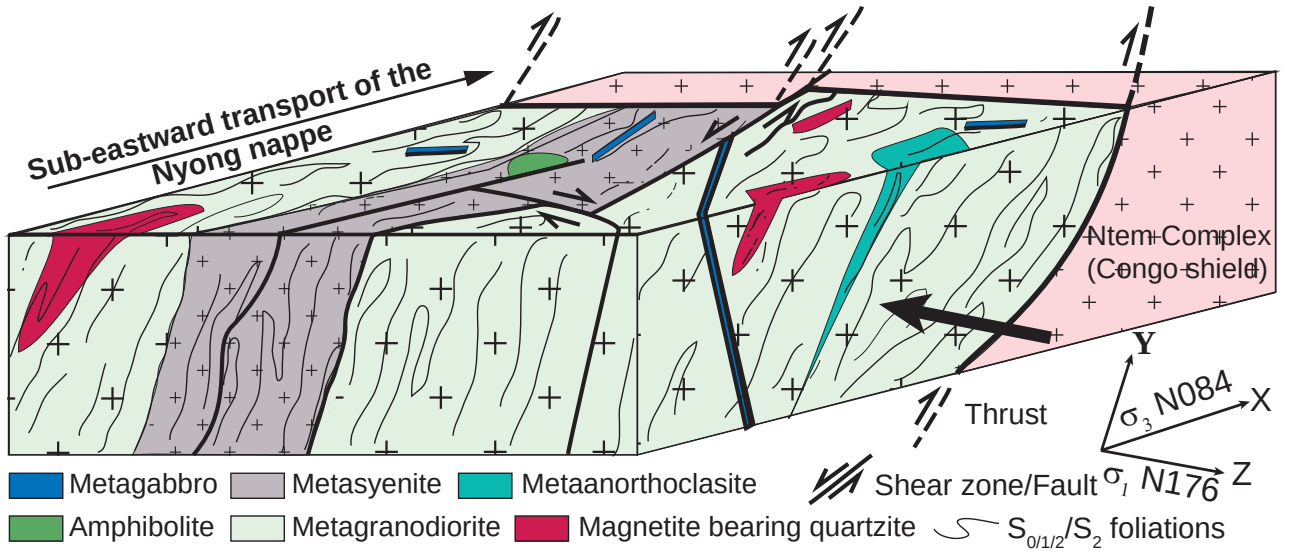

Fig. 9 Schematic 3-D diagram of an interpreted general framework of the eastern part of the Paleoproterozoic Nyong Complex transported top to East onto the Archean Congo shield during the Eburnean/Trans Amazonian orogeny under a general D_2–D_3 transpression regime. D_2 induced by the N176 sub-N–S horizontal shortening (σ_1) and N084 sub-vertical extension (σ_3), emplaced the Nyong tectonic nappe by overprinting and transposing D_1 $S_{0/1}$ foliation into $S_{0/1/2}$ in metasediments coeval to S_2 in meta-granitoids of Archean source, L_2 lineations (N078/30) and F_2 folds associated with the peak of the Eburnean metamorphism. D_3 linked to the Eburnean cooling phase, conferred the ultimate geometry by inducing F_3 folds that affected above foliations and cross-cutting the Nyong nappe by C_3 blastomylonitic shear zones. Various types of lithoclases dissected the area during Proterozoic time.

(2002) and Kurse et al. (2001). The quartz grain boundary area reduction (Fig. 5a), feldspar grain boundary migrations (Figs 5b, c), and the amphibole fish structure (Fig. 5d) indicate that of D_3 operated under amphibolite conditions too (Owona et al. 2013). The Ser ± Cal ± Ep mineral paragenesis indicates greenschist facies reached during the uplift cooling-phase.

We interpret all lithoclases as belonging to D_4. Tension gashes, tension fractures, and faults oriented NE–SW, NNE–SSW, ENE–WSW, and E–W (Figs 2, 7a, b). This indicates both their anachronism and complicated nature (Angelier 1994; Piquer et al. 2016; Sato 2016; Liu et al. 2017; Labuza et al. 2018). Tension gashes represent last magmatic events emplaced under extensional regime contrarily to tension fractures. Reverse dip-slip and vertical strike-slip, dextro- and sinistral-normal faults correspond to dry brittle tectonic features linkable to shortening and extensional tectonic regime (Fig. 7; Piquer et al. 2016; Sato 2016; Liu et al. 2017; Labuza et al. 2018). These are corroborated by multiple σ_1, σ_2 and σ_3 principal stress axes for multiple origins and certainly. The nature of the above feature indicates the post-orogenic character of D_4 (Fig. 2).

Our new $^{207}Pb/^{206}Pb$ zircon data did not reveal any Paleoproterozoic and Eburnean ages in the NyC as found by, e.g., Toteu et al. (1994) Lerouge et al. (2006), Loose and Schenk (2018). This can be related to the measurement of old zircon specimens (Tab. 1, Fig. 8). On the contrary, they support the NyC origin from the Archean NW Congo shield remobilization during its collision with the Sao Francisco shield associated with the Eburnean/Trans Amazonian orogeny (Toteu et al. 1994; Feybesse et al. 1998). This supposes that NyC rocks derived from Archean protoliths. Such Archean inheritance were established in NyC metasyenites at ~2836 Ma (U–Pb zircon, Lerouge et al. 2006). Our new NyC Pb–Pb zircon ages on metagranodiorite and metasyenites that range between 2816–2764 Ma are consistent with those obtained from Edea gneiss with ages between 3174–2519 Ma (Pb/Pb zircon, Lerouge et al. 2006). They are older to Nyong magnetite bearing quartzite of 2776 ± 34 Ma (SHRIMP U–Pb zircon, Lerouge et al. 2006) and 2699 ± 7 Ma (SHRIMP U–Pb zircon; Chombong et al. 2017). They are reliable to 3245–2526 Ma in Ndjole sandstone in the Paleoproterozoic Franceville and Ogoué complexes in Gabon (Pb/Pb zircon, Feybesse et al. 1998). Typical Paleoproterozoic ages from the Nyong ortho- and para-derived rocks linked to the Eburnean/Trans Amazonian orogeny range between ~2100–2000 Ma (TIMS U–Pb zircon, Toteu et al. 1994; SHRIMP U–Pb zircon, Loose and Schenk 2018; SHRIMP U–Pb zircon, Lerouge et al. 2006) as in the whole West Central African Fold belt, notably in Otoumbi-Abamie orthogneiss (Pb/Pb zircon, Feybesse et al. 1998).

We can, therefore, conclude that the NyC in the chrono-litho-structural point of views, consists of deep-seated Archean rocks, exhumed under the diapiric regime, then evolved and end under a transpression flow regimes from various depths that all produced the Paleoproterozoic Nyong fold-and-thrust belts between colliding Congo-San

Francisco shields during the Eburnean/trans Amazonian orogeny. This geodynamic evolution is conceptualized in a 3-D synthetic model shown in Fig. 9.

6. Conclusions

The study of the Ngomedzap–Akongo aimed to constrain the chrono-litho-structural evolution as the eastern part of the NyC, part of the WCAFB. It appears at the end that this area consists of magnetite bearing quartzite, metagranodiorite, meta-anorthoclasite, metasyenite, and metagabbro. They recorded a polyphase D_1–D_3 Eburnean/Trans-Amazonian deformation associated with the collision between the Congo and Sao-Francisco shields (2400–1800 Ma). D_1 phase predominantly a pure shear deformation has been strongly overprinted by dominantly D_2 transpression and horizontal flow regimes that emplaced the Nyong nappe, transported top-to the East onto the Congo shield. This nappe was dissected by D_3 blastomylonitic shear-zones. The D_4 typifies the brittle and post-orogenic phase. Ages obtained with the $^{207}Pb/^{206}Pb$ zircon dating at 2760 ± 26 Ma in metagranodiorite, 2792 ± 13 Ma and 2794 ± 34 Ma metasyenite confirm the Archean origin of the NyC protoliths. The Ngomedzap–Akongo chrono-litho-structural characteristics show that the NyC includes deep-seated Archean protoliths, exhumed from various depths that have formed the Nyong fold-and-thrust belts between colliding Congo-San Francisco shields during the Eburnean/trans Amazonian orogeny.

Acknowledgments Authors are indebted to the DAAD (German Academic Exchange Service) for the financial support at the TU-Bergakademie Freiberg (Germany), and reviewers for constructive suggestions. Special thanks go to the Editor-in-Chief for the careful editorial handling.

References

Abdelsalam GM, Lieges L, Stern RJ (2002) The Saharan Metacraton. J Afr Earth Sci 34: 119–136

Aguilar C, Alkmim FF, Lana C, Farina F (2017) Paleoproterozoic assembly of the São Francisco craton, SE Brazil: New insights from U–Pb titanite and monazite dating. Precambr Res 289: 95–115

Angelier J (1994) Faults slips analysis and paleostress reconstruction. In: Hancock PL (Ed) Continental deformation. Univ. Bristol U.K. Pergamon Press, pp 53–77

Balé P, Brun JP (1989) Late Precambrian thrust and wrench zones in northern Brittany (France). J Struct Geol 11: 391–405

Baratoux L, Metelka V, Naba S, Jessell MW, Gregoire M, Ganne J (2011) Juvenile Paleoproterozoic crust evolution during the Eburnean orogeny (~2.2–2.0 Ga), western Burkina Faso. Precamb Res 191: 18–45

Bédard J (2006) A catalytic delamination-driven model for coupled genesis of Archean crust and sub-continental lithospheric mantle. Geoch Cosm Acta 70: 1188–1214

Bonhomme MG, Gauthier-Lafaye F, Weber F (1982) An example of Lower Proterozoic sediments: the Francevillian in Gabon. Precambr Res 18: 87–102

Boniface N, Schenk V, Appel P (2012) Paleoproterozoic eclogites of MORB-type chemistry and three Proterozoic orogenic cycles in the Ubendian Belt (Tanzania): Evidence from monazite and zircon geochronology, and geochemistry. Precambr Res 192–195: 16–33

Caen-Vachette M, Vialette Y, Bassot JP, Vidal P (1988) Apport de la géochronologie à la connaissance de la géologie gabonaise. Chron Recherche Min 491: 35–54

Carreras J, Druguet E (2018) Complex fold patterns developed by progressive deformation. J Struct Geol 125: 195–201

Castaing C, Feybesse JL, Thieblemont D, Triboulet C, Chevremont P (1994) Paleogeographical reconstructions of the Pan-African/Brasiliano orogen: closure of an oceanic domain or intracontinental convergence between major blocks. Precambr Res 69: 327–344

Chardon D, Gapais D, Cagnard F (2009) Flow of ultra-hot orogens: a view from the Precambrian, clues for the Phanerozoic. Tectonophys 477: 105–118

Chardon D, Jayananda M (2008) Three-dimensional field perspective on deformation, flow, and growth of the lower continental crust (Dharwar craton, India). Tectonics 27: TC1014

Chombong NN, Suh CE, Lehmann B, Vishiti A, Ilouga DC, Shemang EM, Tantoh BS, Kedia AC (2017) Host rock geochemistry, texture and chemical composition of magnetite in iron ore in the Neoarchaean Nyong unit in southern Cameroon. Appl Earth Sci 126: 129–145

Choukroune P, Bouhallier H, Arndt NT (1995) Soft lithosphere during periods of Archean crustal growth or crustal reworking. In: Coward MP, Riess AC (eds) Early Precambrian Processes. Geological Society, London, Special Publications 95, pp 67–86

de Wit MJ, Stankiewicz J, Reeves C (2008) Restoring Pan-African-Brasiliano connections: more Gondwana control, less Trans-Atlantic corruption. In: Pankurst RJ, Trouw RAJ, Brito Neves BB, de Wit MJ (eds) West Gondwana: Pre-Cenozoic correlations across the South Atlantic region. Geological Society, London, Special Publications 294, pp 399–412

Ernst WG (1974) Metamorphism and Ancient Continental Margins. In: Burk CA, Drake CL (eds) The Geology of Continental Margins. Springer, Berlin, Heidelberg, pp 907–919

Feybesse JL, Johan V, Triboulet C, Guerrot C, Mayaga-Minkolo F, Bouchot V, Eko N'dong J (1998) The West

Central African belt: a model of 2.5–2.0 Ma accretion and two-phase orogenic evolution. Precambr Res 87: 161–216

Fossen H, Cavalcante GGC, Pinheiro LRV, Archanjo JC (2018) Deformation – Progressive or multiphase? J Struct Geol 125: 82–99

Gapais D, Cagnard F, Gueydan F, Barbey P, Ballèvre M (2009) Mountain building and exhumation processes through time: inferences from nature and models. Terra Nova 21: 188–194

Hamilton WB (2011) Plate tectonics began in Neoproterozoic time, and plumes from deep mantle have never operated. Lithos 123: 1–20

Houketchang Bouyo M, Pénaye J, Mouri H, Toteu SF (2019) Eclogite facies metabasites from the Paleoproterozoic Nyong Group, SW Cameroon: Mineralogical evidence and implications for a high-pressure metamorphism related to a subduction zone at the NW margin of the Archean Congo craton. J Afr Earth Sci 149: 215–234

Kober B (1987) Single zircon evaporation combined with Pb? emitter bedding for $^{207}Pb/^{206}Pb$-age investigations thermal ion mass spectrometry, and implications to zirconology. Contrib Mineral Petrol 96: 63–71

Kooijman E, Smit M, Ratschbacher L, Kylander-Clarkd ARC (2017) A view into crustal evolution at mantle depths. Earth Planet Sci Lett 465: 59–69

Kurse R, Stünitz H, Kunze K (2001) Dynamic recrystallization processes in plagioclase porphyroclasts. J Struct Geol 23: 1781–1802

Labuza JF, Zeng F, Makhnenko R, Lid Y (2018) Brittle failure of rock: A review and general linear criterion. J Struct Geol 112: 7–28

Ledru P, Johan V, Milési JP, Tegyey M (1994) Markers of the last stages of the Palaeoproterozoic collision: evidence for a 2 Ga continent involving circum-South Atlantic provinces. Precambr Res 69: 169–191

Lerouge C, Coherie A, Toteu SF, Pénaye J, Milesi JP, Tchameni R, Nsifa EN, Fanny MC, Deloule E (2006) Shrimp U–Pb zircon age evidence for Paleoproterozoic sedimentation and 2.05 Ga syntectonic plutonism in the Nyong Group, south-western Cameroon: conse-quences for the Eburnean–Transamazonian belt of NE Brazil and Central Africa. J Afr Earth Sci 44 (4–5): 413–427

Liu Y, Wu K, Wang X, Liu B, Guo J, Du Y (2017) Architecture of buried reverse fault zone in the sedimentary basin: A case study from the Hong-Che Fault Zone of the Junggar Basin. J Struct Geol 105: 1–17

Loose D, Schenk V (2018) 2.09 Ga old eclogites in the Eburnean-Transamazonian orogeny of southern Cameroon: Significance for a Paleoproterozoic plate tectonics. Precambr Res 304: 1–11

Lopez R, Cameron KL, Jones NW (2001) Evidence for Paleoproterozoic, Grenvillian, and Pan-African age Gondwanan crust beneath northeastern Mexico. Precambr Res 107: 195–214

Ludwig KR (2001) User manual for Isoplot/Ex rev 2.49 A geochronological toolkit for Microsoft Excel. Berkeley Geochron Center, Spec Pub 1a, pp 1–55

Maurizot P, Abessolo A, Feybesse A Johan JL, Lecompte P (1986) Etude et prospection minière au Sud-Ouest Cameroun. Synthèse des travaux de 1978–1985. Report BRGM, 85 CNRS 066, Orléans

Miyashiro A (1973) Paired and uparied metamorphic Belts. Tectonophys 17: 241–254

Mvondo H, Lentz D, Bardoux MC (2017) Crustal shortening and thickening in Neoarchean granite-greenstone belts: A case study from the link between the ~2.7 Ga Elu and Hope Bay belts, northeast Slave craton, Canada. J Struct Geol 104: 6–20

Nakapelyukha M, Bubniak I, Bubniak A, Jonckheere R, Ratschbacher L (2018) Cenozoic structural evolution, thermal history, and erosion of the Ukrainian Carpathians fold-thrust belt. Tectonophys 722: 197–209

Nédélec A, Minyem D, Barbey P (1993) High P-High T anatexis of Archean tonalitic grey gneisses: the Eseka migmatites, Cameroon. Precambr Res 62: 191–205

Neves SP, Bruguier O, Vauchez A, Bosch D, Rangel da Silva JM, Mariano G (2006) Timing of crust formation, deposition of supracrustal sequences, and Transamazonian and Brasiliano metamorphism in the East Pernambuco belt (Borborema Province NE Brazil): Implications for western Gondwana assembly. Precambr Res 149: 197–216

Nzenti JP, Barbey P, Macaudiere J, Soba D (1988) Origin and evolution of the late Precambrian high-grade Yaounde gneisses (Cameroon). Precambr Res 38: 91–109

Oba AO (2001) Stratigraphy of Sergipe-alagoas (Brazil), Douala, Rio Muni, and Gabon (West Africa) Sedimentary Basins (Aptian-albian Interval). Columbia, S.C. Dep. Geol. Sci. Univ. South Carolina, pp 16

Oliveira EP, Toteu SF, Araújo MNC, Carvalho MJ, Nascimento RS, Bueno JF, McNaughton N, Basilici G (2006) Geologic correlation between the Neoproterozoic Sergipano belt (NE Brazil) and the Yaounde belt (Cameroon, Africa). J Afr Earth Sci 44 (4–5): 470–478

Omori Y, Barresi A, Kimura N, Okamoto A, Masuda T (2016) Contrast in stressestrain history during exhumation between high- and ultrahigh-pressure metamorphic units in the Western Alps: Microboudinage analysis of piemontite in metacherts. J Struct Geol 89: 169–180

Owona S (2008) Archaean, Eburnean and Pan-African Features and Relationships in Their Junction Zone in the South of Yaounde (Cameroon). Ph.D Thesis, Univ Douala, pp 1–232

Owona S, Mvondo Ondoa J, Ekodeck GE (2013) Evidence of quartz, feldspar and amphibole crystal plastic deformations in the Paleoproterozoic Nyong complex shear zones under amphibolite to granulite conditions (West Central African Fold Belt, SW Cameroon). J Geogr Geol 5(3): 186–201

Owona S, Mvondo Ondoa J, Ratschbacher L, Mbola Ndzana SP, Tchoua MF, Ekodeck GE (2011) The geometry of the Archean, Paleo- and Neoproterozoic tectonics in the Southwest Cameroon. Compt R Geosci 343: 312–322

Passchier CW, Trouw RAJ (2005) Microtectonics. Springer Science & Business Media, pp 1–366

Pénaye J, Toteu SF, Tchameni R, Van Scmus WR, Tchakounté J, Ganwa A, Minyem D, Nsifa EN (2004) The 2.1 Ma West Central African Belt in Cameroon: extension and evolution. J Afr Earth Sci 39: 159–164

Pfiffner O (2006) Thick-skinned and thin-skinned styles of continental contraction. Geol Soc America Special Paper 414: 153–177

Piquer J, Berry RF, Scott RJ, Cooke DR (2016) Arc-oblique fault systems: their role in the Cenozoic structural evolution and metallogenesis of the Andes of central Chile. J Struct Geol 89: 101–117

Price RA (1981) The Cordilleran foreland thrust and fold belt in the southern Canadian Rocky Mountains. Geol Soc London, Special Publications 9(1): 427–448

Ratschbacher L, Hacker BR, Calvert A, Webb EL, Grimmer CJ, McWilliams OM, Ireland T, Dong S, Hu J (2003) Tectonics of the Qinling (Central China): tectonostratigraphy, geochronology, and deformation history. Tectonophys 366: 1–53

Saha-Fouotsa AN, Vanderhaeghe O, Barbey P, Eglinger A, Tchameni R, Zeh A, Tchunte PF, Nomo EN (2019) The geologic record of the exhumed root of the Central African Orogenic Belt in the central Cameroon domain (Mbé – Sassa-Mbersi region). J Afr Earth Sci 151: 286–314

Sanderson DJ, Marchini WR (1984) Transpression. J Struct Geol 6: 449–458

Sato K (2016) A computerized method to estimate friction coefficient from orientation distribution of meso-scale faults. J Struct Geol 89: 44–53

Shang CK, Wolfgang S, Muharrem S, Funken C, Mvondo Ondoa J (2004) Zircon Pb-Pb and U-Pb systematics of TTG rocks in the Congo Craton: constraints on crust formation, magmatism, and Pan-African lead loss. Bull Geosci 79(4): 205–219

Sperner B, Ratschbacher L (1994) A Turbo Pascal program package for graphical presentation and stress analysis of calcite deformation. Z Dtsch geol Gesell 145: 414– 423

Stacey JS, Kramers JD (1975) Approximation of terrestrial lead isotope evolution by a two-stage model. Earth Plan Sci Lett 26: 207–221

Stipp M, Stünitz H, Heilbronner R, Schmid SM (2002). The eastern Tonale fault zone: a 'natural laboratory' for crystal plastic deformation of quartz over a temperature range from 250 to 700 °C. J Struct Geol 24(3): 1861–1884

Tamfu SF, Batupe M, Pauken RJ, Boatwright DC (1995) Geological setting, stratigraphy and hydrocarbon habitat of the Douala Basin. Cameroon. Amer Assoc Petr Geol Bull 79 (13), p 1–95

Tchameni R, Mezger K, Nsifa NE, Pouclet A (2001) Crustal origin of Early Proterozoic syenites in the Congo craton (Ntem complex), South Cameroon. Lithos 57: 23–42

Tikoff B, Fossen H (1995) The limitations of three-dimensional kinematic vorticity analysis. J Struct Geol 17: 1771–1784

Tikoff, Teyssier C (1994) Strain modeling of displacement-field partitioning in transpressional orogens. J Struct Geol 16: 1575–1588

Toteu SF, Van Schmus WR, Pénaye J, Nyobé JB (1994) U/Pb and SM/Nd evidence for Eburnean and Pan-African high-grade metamorphism in cratonic rocks of southern of Cameroon. Precambr Res 67: 321–347

Trompette R (1994) Geology of western Gondwana (2000–500 Ma) Pan-African-Braziliano aggregation of South America and Africa. AA Balkema, Rotterdam, Brookfield, p 350

Vanderhaeghe O, Ledru L, Thiéblemont, Egal E, Cocherie A, Tegyey M, Milési Jean-Pierre (1998) Contrasting mechanism of crustal growth geodynamic evolution of the Paleoproterozoic granite–greenstone belts of French Guiana. Precambr Res 92:165–193

Vanderhaeghe O (2012) The thermal–mechanical evolution of crustal orogenic belts at convergent plate boundaries: A reappraisal of the orogenic cycle. J Geodyn 56–57: 124–145

Vicat JP, Léger JM, Nsifa KE, Piguet P, Nzenti JP, Tchameni R, Pouclet A (1996) Distinction au sein du craton congolais du Sud-Ouest du Cameroun, de deux épisodes doléritiques initiant les cycles orogéniques éburnéen (Paléoprotérozoique) et panafricain (Néoprotérozoique). C R Acad Sci, Paris, 323 (IIa): 575–582

Vicat JP, Pouclet A (1995) Nature du magmatisme lié à une extension pré-panafricaine: les dolérites des bassins de Comba et de Sembé-Ouesso. Bull Soc Géol Fr 166 (4): 355–364

Vicat JP, Pouclet A, Nkoumbou C, Sémé Mouangue A (1997) Le volcanisme fissural néoprotérozoïque du Dja inférieur, de Yokadouma (Cameroun) et de Nola (RCA)-Signification géotectonique. The fissural Neoproterozoic volcanism of the Lower Dja, Yokadouma (Cameroon) and Nola (RCA) series-Geotectonic meaning. C R Acad Sci, Paris, 325: 671–677

Wiedenbeck M, Alle P, Corfu F, Griffin WL, Meier M, Oberli F, von Quadt A, Roddick JC, Spiegel W (1995) Three natural zircon standards for U–Th–Pb, Lu–Hf, trace element and REE analysis. Geost Newsletter 19: 1–23

William PF, Goodwin BL, Ralser S (1994) Ductile deformation processes. In: Hancock Pl (ed) Continental deformation. Univ Bristol, UK. Pergamon Press, pp 1–27